Search for Anomalous Photonic Events with Missing Energy in e$^+$e$^-$ Collisions at $\sqrt{s} = 130$, 136 and 183 GeV

The OPAL Collaboration

Abstract

Photonic events with large missing energy have been observed in e$^+$e$^-$ collisions at centre-of-mass energies of 130, 136 and 183 GeV collected in 1997 using the OPAL detector at LEP. Results are presented for event topologies with a single photon and missing transverse energy or with an acoplanar photon pair. Cross-section measurements are performed within the kinematic acceptance of each selection. These results are compared with the expectations from the Standard Model process e$^+$e$^- \rightarrow \nu\overline{\nu}$ + photon(s). No evidence is observed for new physics contributions to these final states. Using the data at $\sqrt{s} = 183$ GeV, upper limits on $\sigma(\text{e}^+\text{e}^- \rightarrow \text{XY}) \cdot \text{BR}(\text{X} \rightarrow \text{Y}\gamma)$ and $\sigma(\text{e}^+\text{e}^- \rightarrow \text{XX}) \cdot \text{BR}^2(\text{X} \rightarrow \text{Y}\gamma)$ are derived for the case of stable and invisible Y. These limits apply to single and pair production of excited neutrinos (X = ν^*, Y = ν), to neutralino production (X = $\tilde{\chi}_2^0$, Y = $\tilde{\chi}_1^0$) and to supersymmetric models in which X = $\tilde{\chi}_1^0$ and Y = $\tilde{\text{G}}$ is a light gravitino.

(Submitted to Eur. Phys. J. **C**.)

The OPAL Collaboration

G. Abbiendi[2], K. Ackerstaff[8], G. Alexander[23], J. Allison[16], N. Altekamp[5], K.J. Anderson[9],
S. Anderson[12], S. Arcelli[17], S. Asai[24], S.F. Ashby[1], D. Axen[29], G. Azuelos[18,a], A.H. Ball[17],
E. Barberio[8], R.J. Barlow[16], R. Bartoldus[3], J.R. Batley[5], S. Baumann[3], J. Bechtluft[14], T. Behnke[27],
K.W. Bell[20], G. Bella[23], A. Bellerive[9], S. Bentvelsen[8], S. Bethke[14], S. Betts[15], O. Biebel[14], A. Biguzzi[5],
S.D. Bird[16], V. Blobel[27], I.J. Bloodworth[1], M. Bobinski[10], P. Bock[11], J. Böhme[14], D. Bonacorsi[2],
M. Boutemeur[34], S. Braibant[8], P. Bright-Thomas[1], L. Brigliadori[2], R.M. Brown[20], H.J. Burckhart[8],
C. Burgard[8], R. Bürgin[10], P. Capiluppi[2], R.K. Carnegie[6], A.A. Carter[13], J.R. Carter[5], C.Y. Chang[17],
D.G. Charlton[1,b], D. Chrisman[4], C. Ciocca[2], P.E.L. Clarke[15], E. Clay[15], I. Cohen[23], J.E. Conboy[15],
O.C. Cooke[8], C. Couyoumtzelis[13], R.L. Coxe[9], M. Cuffiani[2], S. Dado[22], G.M. Dallavalle[2], R. Davis[30],
S. De Jong[12], L.A. del Pozo[4], A. de Roeck[8], K. Desch[8], B. Dienes[33,d], M.S. Dixit[7], J. Dubbert[34],
E. Duchovni[26], G. Duckeck[34], I.P. Duerdoth[16], D. Eatough[16], P.G. Estabrooks[6], E. Etzion[23],
H.G. Evans[9], F. Fabbri[2], M. Fanti[2], A.A. Faust[30], F. Fiedler[27], M. Fierro[2], I. Fleck[8], R. Folman[26],
A. Fürtjes[8], D.I. Futyan[16], P. Gagnon[7], J.W. Gary[4], J. Gascon[18], S.M. Gascon-Shotkin[17],
G. Gaycken[27], C. Geich-Gimbel[3], G. Giacomelli[2], P. Giacomelli[2], V. Gibson[5], W.R. Gibson[13],
D.M. Gingrich[30,a], D. Glenzinski[9], J. Goldberg[22], W. Gorn[4], C. Grandi[2], E. Gross[26], J. Grunhaus[23],
M. Gruwé[27], G.G. Hanson[12], M. Hansroul[8], M. Hapke[13], K. Harder[27], C.K. Hargrove[7], C. Hartmann[3],
M. Hauschild[8], C.M. Hawkes[5], R. Hawkings[27], R.J. Hemingway[6], M. Herndon[17], G. Herten[10],
R.D. Heuer[8], M.D. Hildreth[8], J.C. Hill[5], S.J. Hillier[1], P.R. Hobson[25], A. Hocker[9], R.J. Homer[1],
A.K. Honma[28,a], D. Horváth[32,c], K.R. Hossain[30], R. Howard[29], P. Hüntemeyer[27], P. Igo-Kemenes[11],
D.C. Imrie[25], K. Ishii[24], F.R. Jacob[20], A. Jawahery[17], H. Jeremie[18], M. Jimack[1], C.R. Jones[5],
P. Jovanovic[1], T.R. Junk[6], D. Karlen[6], V. Kartvelishvili[16], K. Kawagoe[24], T. Kawamoto[24],
P.I. Kayal[30], R.K. Keeler[28], R.G. Kellogg[17], B.W. Kennedy[20], A. Klier[26], S. Kluth[8], T. Kobayashi[24],
M. Kobel[3,e], D.S. Koetke[6], T.P. Kokott[3], M. Kolrep[10], S. Komamiya[24], R.V. Kowalewski[28], T. Kress[11],
P. Krieger[6], J. von Krogh[11], T. Kuhl[3], P. Kyberd[13], G.D. Lafferty[16], D. Lanske[14], J. Lauber[15],
S.R. Lautenschlager[31], I. Lawson[28], J.G. Layter[4], D. Lazic[22], A.M. Lee[31], D. Lellouch[26], J. Letts[12],
L. Levinson[26], R. Liebisch[11], B. List[8], C. Littlewood[5], A.W. Lloyd[1], S.L. Lloyd[13], F.K. Loebinger[16],
G.D. Long[28], M.J. Losty[7], J. Ludwig[10], D. Liu[12], A. Macchiolo[2], A. Macpherson[30], W. Mader[3],
M. Mannelli[8], S. Marcellini[2], C. Markopoulos[13], A.J. Martin[13], J.P. Martin[18], G. Martinez[17],
T. Mashimo[24], P. Mättig[26], W.J. McDonald[30], J. McKenna[29], E.A. Mckigney[15], T.J. McMahon[1],
R.A. McPherson[28], F. Meijers[8], S. Menke[3], F.S. Merritt[9], H. Mes[7], J. Meyer[27], A. Michelini[2],
S. Mihara[24], G. Mikenberg[26], D.J. Miller[15], R. Mir[26], W. Mohr[10], A. Montanari[2], T. Mori[24], K. Nagai[8],
I. Nakamura[24], H.A. Neal[12], B. Nellen[3], R. Nisius[8], S.W. O'Neale[1], F.G. Oakham[7], F. Odorici[2],
H.O. Ogren[12], M.J. Oreglia[9], S. Orito[24], J. Pálinkás[33,d], G. Pásztor[32], J.R. Pater[16], G.N. Patrick[20],
J. Patt[10], R. Perez-Ochoa[8], S. Petzold[27], P. Pfeifenschneider[14], J.E. Pilcher[9], J. Pinfold[30], D.E. Plane[8],
P. Poffenberger[28], J. Polok[8], M. Przybycień[8], C. Rembser[8], H. Rick[8], S. Robertson[28], S.A. Robins[22],
N. Rodning[30], J.M. Roney[28], K. Roscoe[16], A.M. Rossi[2], Y. Rozen[22], K. Runge[10], O. Runolfsson[8],
D.R. Rust[12], K. Sachs[10], T. Saeki[24], O. Sahr[34], W.M. Sang[25], E.K.G. Sarkisyan[23], C. Sbarra[29],
A.D. Schaile[34], O. Schaile[34], F. Scharf[3], P. Scharff-Hansen[8], J. Schieck[11], B. Schmitt[8], S. Schmitt[11],
A. Schöning[8], M. Schröder[8], M. Schumacher[3], C. Schwick[8], W.G. Scott[20], R. Seuster[14], T.G. Shears[8],
B.C. Shen[4], C.H. Shepherd-Themistocleous[8], P. Sherwood[15], G.P. Siroli[2], A. Sittler[27], A. Skuja[17],
A.M. Smith[8], G.A. Snow[17], R. Sobie[28], S. Söldner-Rembold[10], M. Sproston[20], A. Stahl[3],
K. Stephens[16], J. Steuerer[27], K. Stoll[10], D. Strom[19], R. Ströhmer[34], B. Surrow[8], S.D. Talbot[1],
S. Tanaka[24], P. Taras[18], S. Tarem[22], R. Teuscher[8], M. Thiergen[10], M.A. Thomson[8], E. von Törne[3],
E. Torrence[8], S. Towers[6], I. Trigger[18], Z. Trócsányi[33], E. Tsur[23], A.S. Turcot[9], M.F. Turner-Watson[8],
R. Van Kooten[12], P. Vannerem[10], M. Verzocchi[10], H. Voss[3], F. Wäckerle[10], A. Wagner[27], C.P. Ward[5],
D.R. Ward[5], P.M. Watkins[1], A.T. Watson[1], N.K. Watson[1], P.S. Wells[8], N. Wermes[3], J.S. White[6],
G.W. Wilson[16], J.A. Wilson[1], T.R. Wyatt[16], S. Yamashita[24], G. Yekutieli[26], V. Zacek[18], D. Zer-Zion[8]

[1]School of Physics and Astronomy, University of Birmingham, Birmingham B15 2TT, UK

[2]Dipartimento di Fisica dell' Università di Bologna and INFN, I-40126 Bologna, Italy

[3]Physikalisches Institut, Universität Bonn, D-53115 Bonn, Germany

[4]Department of Physics, University of California, Riverside CA 92521, USA

[5]Cavendish Laboratory, Cambridge CB3 0HE, UK

[6]Ottawa-Carleton Institute for Physics, Department of Physics, Carleton University, Ottawa, Ontario K1S 5B6, Canada

[7]Centre for Research in Particle Physics, Carleton University, Ottawa, Ontario K1S 5B6, Canada

[8]CERN, European Organisation for Particle Physics, CH-1211 Geneva 23, Switzerland

[9]Enrico Fermi Institute and Department of Physics, University of Chicago, Chicago IL 60637, USA

[10]Fakultät für Physik, Albert Ludwigs Universität, D-79104 Freiburg, Germany

[11]Physikalisches Institut, Universität Heidelberg, D-69120 Heidelberg, Germany

[12]Indiana University, Department of Physics, Swain Hall West 117, Bloomington IN 47405, USA

[13]Queen Mary and Westfield College, University of London, London E1 4NS, UK

[14]Technische Hochschule Aachen, III Physikalisches Institut, Sommerfeldstrasse 26-28, D-52056 Aachen, Germany

[15]University College London, London WC1E 6BT, UK

[16]Department of Physics, Schuster Laboratory, The University, Manchester M13 9PL, UK

[17]Department of Physics, University of Maryland, College Park, MD 20742, USA

[18]Laboratoire de Physique Nucléaire, Université de Montréal, Montréal, Quebec H3C 3J7, Canada

[19]University of Oregon, Department of Physics, Eugene OR 97403, USA

[20]CLRC Rutherford Appleton Laboratory, Chilton, Didcot, Oxfordshire OX11 0QX, UK

[22]Department of Physics, Technion-Israel Institute of Technology, Haifa 32000, Israel

[23]Department of Physics and Astronomy, Tel Aviv University, Tel Aviv 69978, Israel

[24]International Centre for Elementary Particle Physics and Department of Physics, University of Tokyo, Tokyo 113-0033, and Kobe University, Kobe 657-8501, Japan

[25]Institute of Physical and Environmental Sciences, Brunel University, Uxbridge, Middlesex UB8 3PH, UK

[26]Particle Physics Department, Weizmann Institute of Science, Rehovot 76100, Israel

[27]Universität Hamburg/DESY, II Institut für Experimental Physik, Notkestrasse 85, D-22607 Hamburg, Germany

[28]University of Victoria, Department of Physics, P O Box 3055, Victoria BC V8W 3P6, Canada

[29]University of British Columbia, Department of Physics, Vancouver BC V6T 1Z1, Canada

[30]University of Alberta, Department of Physics, Edmonton AB T6G 2J1, Canada

[31]Duke University, Dept of Physics, Durham, NC 27708-0305, USA

[32]Research Institute for Particle and Nuclear Physics, H-1525 Budapest, P O Box 49, Hungary

[33]Institute of Nuclear Research, H-4001 Debrecen, P O Box 51, Hungary

[34]Ludwigs-Maximilians-Universität München, Sektion Physik, Am Coulombwall 1, D-85748 Garching, Germany

[a] and at TRIUMF, Vancouver, Canada V6T 2A3

[b] and Royal Society University Research Fellow

[c] and Institute of Nuclear Research, Debrecen, Hungary

[d] and Department of Experimental Physics, Lajos Kossuth University, Debrecen, Hungary

[e] on leave of absence from the University of Freiburg

1 Introduction

We describe measurements and searches using a data sample of photonic events with large missing energy collected in 1997 with the OPAL detector at LEP. The events result from e^+e^- collisions at centre-of-mass energies of 130.0, 136.0 and 182.7 GeV with integrated luminosities of 2.35, 3.37 and 54.5 pb^{-1}, respectively. The present paper complements our recent publication of results from earlier data samples [1] consisting of a total of 25 pb^{-1} at centre-of-mass energies of 130, 136, 161 and 172 GeV. Results on photonic events without missing energy at $\sqrt{s} = 183$ GeV are presented in a separate paper [2]. Recent measurements of photonic event production have also been made by the other LEP collaborations at centre-of-mass energies above the W pair threshold [3], including new results at $\sqrt{s} = 183$ GeV [4]. Related searches in $p\overline{p}$ collisions have been reported in [5]. The interest in the 1997 data is twofold. The main motivation is that the large data set at a higher centre-of-mass energy (183 GeV) gives discovery potential in a new kinematic regime. Additionally, the lower energy data sets allow the experiment at 130 and 136 GeV to be repeated leading to a check of our previous results which indicated an excess of events with acoplanar photons [1].

The single-photon and acoplanar-photons search topologies presented here are designed to select events with one or more photons and significant missing transverse energy, indicating the presence of at least one neutrino-like invisible particle which interacts only weakly with matter. The event selections for these search topologies are similar to those used in our recent publication [1]. The main changes are improvements in the rejection of backgrounds from cosmic ray interactions which allow for an increased kinematic acceptance of the single-photon topology. The single-photon search topology is sensitive to neutral events in which there are one or two photons and missing energy which, within the Standard Model, are expected from the $e^+e^- \rightarrow \nu\overline{\nu}\gamma(\gamma)$ process[1]. The allowance for two observed photons retains acceptance for doubly radiative neutrino pair production. The acoplanar-photons search topology is designed to select neutral events with two or more photons and significant missing transverse energy which, within the Standard Model, are expected from the $e^+e^- \rightarrow \nu\overline{\nu}\gamma\gamma(\gamma)$ process. The selection is designed to retain acceptance for events with three photons, if the system formed by the three photons shows evidence for significant missing transverse energy.

These photonic final-state topologies are sensitive to new physics of the type $e^+e^- \rightarrow XY$ and $e^+e^- \rightarrow XX$ where X is neutral and decays radiatively $(X \rightarrow Y\gamma)$ and Y is stable and only weakly interacting. For the general case of massive X and Y this includes conventional supersymmetric processes [6] $(X = \tilde{\chi}_2^0, Y = \tilde{\chi}_1^0)$. In this context it has been emphasized [7] that the radiative branching ratio of the $\tilde{\chi}_2^0$ may be large. These topologies also have particularly good sensitivity for the special case of $M_Y \approx 0$. This applies both to the production of excited neutrinos $(X = \nu^*, Y = \nu)$ and to supersymmetric models in which the lightest supersymmetric particle (LSP) is a light gravitino[2] and $\tilde{\chi}_1^0$ is the next-to-lightest supersymmetric particle (NLSP) which decays to a gravitino and a photon $(X = \tilde{\chi}_1^0, Y = \tilde{G})$. For supersymmetric models with a light gravitino, the photonic branching ratio of the $\tilde{\chi}_1^0$ is naturally large. Such a signature has been discussed in [8] and more recently in [9–12] in the context of both no-scale supergravity models and gauge-mediated supersymmetry breaking models. Other types of new physics to which these search topologies are sensitive include the production of an invisible particle in association with a photon and the production of invisible particles tagged by initial-state radiation. An example of this is $e^+e^- \rightarrow \tilde{G}\tilde{G}\gamma$ [13]. The acoplanar-photons search topology also has sensitivity to the production of two particles, one invisible, or with an invisible decay mode, and the other decaying into two photons. Such events might arise from the production of a Higgs-like scalar particle, $S^0 : e^+e^- \rightarrow Z^0S^0$, followed by $S^0 \rightarrow \gamma\gamma$, $Z^0 \rightarrow \nu\overline{\nu}$. OPAL results from a search for this process at $\sqrt{s} = 183$ GeV, including the hadronic and leptonic Z^0 decays, are reported

---

[1]The photon in parentheses denotes that the presence of this photon is allowed but not required.
[2]The mass scale is typically $\mathcal{O}(\text{keV})$.

3

in a separate paper [14]. The results from our previous searches [1] for $e^+e^- \to XY$ and $e^+e^- \to XX$ with $X \to Y\gamma$ have been used to set model-dependent limits on excited neutrinos and neutralinos [15]. The new results reported here can be used in the same manner.

This paper will first briefly describe the detector and the Monte Carlo samples used. The event selection for each search topology will then be described, followed by cross-section measurements for $e^+e^- \to \nu\overline{\nu}\gamma(\gamma)$ and $e^+e^- \to \nu\overline{\nu}\gamma\gamma(\gamma)$ and comparisons with Standard Model expectations. Implications of these results on the possibility of new physics processes will be discussed.

2 Detector and Monte Carlo Samples

The OPAL detector, which is described in detail in [16], contains a pressurized central tracking system operating inside a solenoid with a magnetic field of 0.435 T. The region outside the solenoid (barrel) and the pressure bell (endcap) is instrumented with scintillation counters, presamplers and the lead-glass electromagnetic calorimeter (ECAL). The magnet return yoke is instrumented for hadron calorimetry and is surrounded by external muon chambers. Electromagnetic calorimeters close to the beam axis measure luminosity and complete the acceptance.

The measurements presented here are mainly based on the observation of clusters of energy deposited in the lead-glass electromagnetic calorimeter. This consists of an array of 9,440 lead-glass blocks in the barrel ($|\cos\theta| < 0.82$) with a quasi-pointing geometry and two dome-shaped endcap arrays, each of 1,132 lead-glass blocks, covering the polar angle[3] range ($0.81 < |\cos\theta| < 0.984$). Energies measured in the ECAL will normally refer to those obtained after corrections to account for losses in upstream material. Energies without these corrections are called deposited energies. In the regions ($0.72 < |\cos\theta| < 0.82$) and ($|\cos\theta| > 0.945$), the energy resolution of the ECAL is degraded relative to the nominal resolution. This degradation is largely due to increased amounts of material in front of the ECAL. In some cases (where stated) these regions have been excluded from the analysis. Fully hermetic electromagnetic calorimeter coverage is achieved beyond the end of the ECAL down to small polar angles with the use of the the gamma-catcher calorimeter, the forward calorimeter (FD) and the silicon-tungsten calorimeter (SW). These detectors cover the angular regions with respect to the beam of 140-205 mrad, 40-145 mrad and 24-59 mrad, respectively. However, a small region centred on a polar angle of 30 mrad lacks useful calorimetric coverage due to the installation, in 1996, of a thick tungsten shield designed to protect the tracking chambers from synchrotron radiation background. The effective limit of electromagnetic hermeticity is therefore around 33 mrad.

Scintillators in the barrel and endcap regions are used to reject backgrounds from cosmic ray interactions and to provide time measurements for the large fraction ($\approx 80\%$) of photons which convert in the material in front of the ECAL. The barrel time-of-flight (TOF) scintillator bars are located outside the solenoid in front of the barrel ECAL and match its geometrical acceptance ($|\cos\theta| < 0.82$). Arrays of thin scintillating tiles with embedded wavelength-shifting-fibre readout [17] were installed prior to the 1997 run. The new tile endcap (TE) scintillator arrays are located at $0.81 < |\cos\theta| < 0.955$ behind the pressure bell and in front of the endcap ECAL.

Additional scintillating tile arrays, referred to as the MIP-PLUG, were installed at polar angles between 40 and 200 mrad and consist of two pairs of scintillating tile layers designed for detection of muons. The outer pair, covering the angular range of 125 to 200 mrad is used in this paper to provide

---

[3]In the OPAL coordinate system, θ is the polar angle defined with respect to the electron beam direction and ϕ is the azimuthal angle.

redundancy in the rejection of events with energetic electromagnetic showers in the gamma-catcher region.

The tracking system, consisting of a silicon microvertex detector (SI), a vertex drift chamber (CV) and a large volume jet drift chamber (CJ), is used to reject events with prompt charged particles. The silicon microvertex detector consists of two concentric cylindrical layers of silicon microstrip arrays, each layer providing both an azimuthal and longitudinal (along the beam direction) coordinate measurement. The two-layer acceptance covers $|\cos\theta| < 0.90$.

Beam related backgrounds and backgrounds arising from cosmic ray interactions are rejected using the scintillator timing measurements and information from the electromagnetic calorimeter shower shape, the hadron calorimeter and the muon detectors. The integrated luminosities of the data samples are determined to better than 1% from small-angle Bhabha scattering events in the SW calorimeter. Triggers [18] based on electromagnetic energy deposits in either the barrel or endcap electromagnetic calorimeters, and also on a coincidence of energy in the barrel electromagnetic calorimeter and a hit in the TOF system, lead to full trigger efficiency for photonic events passing the event selection criteria described in the following section.

For the expected Standard Model signal process, $e^+e^- \rightarrow \nu\overline{\nu} + \text{photon(s)}$, the Monte Carlo generator KORALZ [19] was used. For other expected Standard Model processes, a number of different generators were used: RADCOR [20] for $e^+e^- \rightarrow \gamma\gamma(\gamma)$; BHWIDE [21] and TEEGG [22] for $e^+e^- \rightarrow e^+e^-(\gamma)$; grc4f [23] for $e^+e^- \rightarrow \ell^+\ell^-\nu\bar{\nu}(\gamma)$; and KORALZ for $e^+e^- \rightarrow \mu^+\mu^-(\gamma)$ and $e^+e^- \rightarrow \tau^+\tau^-(\gamma)$. The expected contributions from each of these Standard Model processes were evaluated using a total equivalent integrated luminosity at least ten times larger than the integrated luminosity of the data sample.

To simulate possible new physics processes of the type $e^+e^- \rightarrow XY$ and $e^+e^- \rightarrow XX$ where X decays to $Y\gamma$ and Y escapes detection, a modified version of the SUSYGEN [24] Monte Carlo generator was used to produce neutralino pair events of the type $e^+e^- \rightarrow \tilde{\chi}_2^0\tilde{\chi}_1^0$ and $e^+e^- \rightarrow \tilde{\chi}_2^0\tilde{\chi}_2^0$, $\tilde{\chi}_2^0 \rightarrow \tilde{\chi}_1^0\gamma$, with isotropic angular distributions for the production and decay of $\tilde{\chi}_2^0$ and including initial-state radiation. Monte Carlo events were generated at 40 (for XY production) and 42 (for XX production) points in the kinematically accessible region of the (M_X, M_Y) plane. All the Monte Carlo samples described above were processed through the OPAL detector simulation [25].

3 Photonic Event Selection

This section describes the criteria for selecting single-photon and acoplanar-photons events. The kinematic acceptance of each selection is defined in terms of the photon energy, E_γ, and the photon polar angle, θ. In addition, the scaled energy, x_γ, is defined as E_γ/E_{beam}, and the scaled transverse energy, x_T, as $x_\gamma \sin\theta$.

Single-Photon - One or two photons accompanied by invisible particle(s):

- At least one photon with $x_T > 0.05$ and with $15° < \theta < 165°$ ($|\cos\theta| < 0.966$).

Acoplanar-Photons - Two or more photons accompanied by invisible particle(s):

- At least two photons, each with $x_\gamma > 0.05$ and $15° < \theta < 165°$, or one photon with $E_\gamma > 1.75$ GeV and $|\cos\theta| < 0.8$ and a second photon with $E_\gamma > 1.75$ GeV and $15° < \theta < 165°$.

- The scaled transverse momentum of the two-photon system consisting of the two highest energy photons, $p_T^{\gamma\gamma}$, must satisfy $p_T^{\gamma\gamma}/E_{\text{beam}} > 0.05$.

In each of the two cases, it is desirable to retain acceptance for events with additional photons, if the resulting photonic system is still consistent with the presence of significant missing energy. This reduces the sensitivity of each measurement to the modelling of higher-order contributions. Consequently, a large fraction of the kinematic acceptance of the acoplanar-photons selection is also contained in the kinematic acceptance of the single-photon selection.

3.1   Single-Photon Event Selection

The single-photon selection criteria are similar to the previous OPAL analysis of photonic events with missing energy [1] but have increased acceptance for lower energy photons due to improved rejection and control of cosmic ray and beam related backgrounds. The modifications also improve the efficiency for events with two detected photons.

- **Kinematic acceptance.** Events must contain a primary electromagnetic cluster (that with the highest deposited energy in the barrel or endcap calorimeters) in the region $15° < \theta < 165°$ ($|\cos\theta| < 0.966$) with $x_T > 0.05$. Events are considered to have more than one photon if additional electromagnetic clusters are found in the barrel or endcap calorimeter ($|\cos\theta| < 0.984$) having deposited energy exceeding 300 MeV.

- **Cluster quality.** The primary electromagnetic cluster, combined with any clusters contiguous with it, must be consistent with the cluster size and energy sharing of blocks for a photon coming from near the interaction point. The cluster size varies in both azimuthal and polar angle extent as a function of $|\cos\theta|$. The cluster extent cuts are parametrized in $|\cos\theta|$ accordingly. Events are rejected if the cluster energy exceeds the beam energy by more than three standard deviations.

- **Forward energy vetoes.** Events are rejected if the energy sum of gamma-catcher clusters in either end is greater than 5 GeV. Events are also rejected if either layer of the outer MIP-PLUG shows evidence of an energetic shower (pulse-height exceeding about ten minimum ionizing particle equivalents). An event can also be vetoed based on the transverse momentum sum of clusters measured in the forward calorimeters FD and SW. Events are rejected that have a transverse momentum sum exceeding 1 GeV and where the azimuthal angle of the transverse momentum sum is within 60° in azimuth of the direction opposite the measured momentum of the photonic system. A final complementary veto rejects events that have an energy sum exceeding 5 GeV where the sum is over all clusters in the FD, SW and forward part of the endcap ECAL ($|\cos\theta| > 0.966$) which are within 60° in azimuth of the direction opposite the measured momentum of the photonic system. The directional nature of these last two vetoes removes events with forward going high-energy particles that can account for some or all of the missing transverse momentum. However, it minimizes losses from random noise or accidental energy deposits in the forward detectors. It also allows for the presence of initial-state radiated photons in the forward region which are not back-to-back with the photon(s).

- **Muon veto.** Events are rejected if there are any muon track segments reconstructed in the muon chambers or in the hadron calorimeters. Events are also rejected if there is significant activity in the outer part of the barrel hadron calorimeter. The muon veto is used primarily to remove cosmic ray background.

- **Selective multi-photon veto.** This veto addresses backgrounds, principally from $e^+e^- \to \gamma\gamma(\gamma)$, whilst retaining acceptance for events with two photons and missing energy. Events with a second photon are rejected if any of the following criteria are satisfied:

  - The total energy of the two clusters exceeds $0.9\sqrt{s}$.
  - The acoplanarity angle[4] of the two clusters is less than $2.5°$.
  - The missing momentum vector calculated from the two clusters satisfies $|\cos\theta_{\mathrm{miss}}| > 0.9$.
  - A third electromagnetic cluster is detected with deposited energy exceeding 300 MeV.
  - $p_T^{\gamma\gamma}/E_{\mathrm{beam}} < 0.05$.
  - For events with at least one of the two clusters in the region $|\cos\theta| > 0.95$, the variable b_T is less than 0.1, where $b_T = (\sin\theta_1 + \sin\theta_2)|\cos[(\phi_1 - \phi_2)/2]|$. This amounts to a stronger acoplanarity cut for events with at least one forward photon.
  - Events with an energy sum greater than 1 GeV in either end of FD or SW are rejected if the two-photon plus forward photon system is planar, namely if the sum of the three opening angles exceeds $350°$.

Events are required to either contain no reconstructed charged tracks or contain a photon candidate consistent with a photon conversion observed within the central tracking volume. These events are referred to as non-conversion and conversion candidates, respectively. These two classes are mutually exclusive. We will now describe in turn the additional criteria used for each candidate class.

Non-conversion candidates must satisfy the following additional criteria :

- **Charged track veto.** It is required that there are no reconstructed tracks with 10 or more hits in CJ.

- **Timing requirements.** The criteria depend on the polar angle of the primary cluster. For the angular region $|\cos\theta| < 0.72$, either an in-time associated TOF hit or the absence of the special background vetoes (described below) is required. The second requirement is made in order to retain acceptance for photons that do not convert before reaching the TOF counters. For the range $0.72 < |\cos\theta| < 0.82$, where the muon coverage is not complete and the material in front of the ECAL leads to a high probability of a photon being detected in the TOF, a good in-time associated TOF hit is required. For $|\cos\theta| > 0.82$, a good in-time associated TE hit is required as well as the absence of the first three of the special background vetoes described below. A cluster with an associated TOF (TE) hit is considered to be in-time if the measured arrival time of the photon at the TOF (TE) is within 5 (30) ns of the expected time for a photon originating from the interaction point. These definitions of in-time hits also apply to the single-photon conversion selection as well as the acoplanar-photons selection. Events with a photon candidate having an out-of-time associated TOF or TE hit are rejected as cosmic rays.

- **Special background vetoes.** Three special background vetoes are used for candidates that are in the endcap region or that have no TOF timing information. A fourth special background veto is used only for photon candidates with $|\cos\theta| < 0.72$ that have no TOF timing information. The first veto rejects events in which any of the three muon triggers [18] (barrel and two endcaps) were present. This veto rejects cosmic ray background. The second looks for a series of electromagnetic or hadronic calorimeter clusters consistent with the same radial and azimuthal position as the primary cluster, but at different positions along the beam direction. This veto rejects beam halo

---

[4]Defined as $180°$ minus the opening angle in the transverse plane.

backgrounds. The third looks for a series of hits in the outer layers of the hadron calorimeter. This veto rejects both cosmic rays and beam related backgrounds. The fourth veto is based on the shape of the cluster in the barrel ECAL. The observed energy deposition in each lead-glass block of the cluster is fitted to the expected shower profile for a photon coming from the interaction point. One then calculates the variable S (in radiation lengths), defined as the difference between the measured and expected values of the energy-weighted lateral distance from the fitted shower centroid. Events with S exceeding 0.2 are rejected. This veto rejects cosmic rays and beam related backgrounds, both of which tend to have shower shapes wider than those of photons originating from the interaction point.

Conversion candidates must satisfy the following additional criteria :

- **Photon conversion consistency.** There must be at least one reconstructed charged track in the central tracking chambers. The charged track with the most hits must be associated in space to at least one of the two most energetic photon candidates. In particular, the measured polar angle of the track should be consistent with the polar angle of the ECAL cluster to within 100 mrad, and the azimuth at the point of closest approach of the track to the interaction point should differ by less than 100 mrad from the measured azimuthal angle of the ECAL cluster. The azimuthal matching criterion is relaxed to 500 mrad for clusters with $|\cos\theta| > 0.90$ since conversions at forward angles often lead to large showers and difficulties in resolving the jet chamber left-right ambiguity. In addition, for such forward photon conversion candidates, which mostly convert in the CV endplate, it was further required that there be at least 12 out of the first 16 wires hit in CJ.

- **Prompt charged track veto.** Events are rejected as being consistent with containing a prompt charged track if at least one photon candidate has azimuthally associated hits in the innermost tracking detector (SI for $|\cos\theta| < 0.9$ and CV otherwise).

- **Two or more track veto.** Events with conversion candidates are rejected if they have at least two tracks, reconstructed from axial-wire hits in CV, with an opening angle in the transverse plane exceeding 45°. This criterion is used principally for redundancy in the rejection of Bhabha scattering events.

- **Identified cosmic ray veto.** Events with at least two electromagnetic clusters in the barrel region each with associated TOF hits are rejected as identified cosmic rays if the time difference between the upper and lower TOF hits is consistent with a downward-going cosmic ray.

- **Timing requirements.** The photon(s) associated with the track is required to have an in-time TOF or TE hit depending on whether the polar angle of the photon matches the TOF or TE geometrical acceptance.

Distributions of some quantities used in the event selection are illustrated in Figures 1 and 2. For photons with $|\cos\theta| < 0.82$, Figure 1a shows the difference between the measured TOF timing and that expected for a photon originating from the interaction point for events passing all selection criteria or failing only the TOF timing requirement. The eleven events outside the accepted region of ±5 ns are rejected as cosmic rays. The expected region for good events is shown in greater detail in Figure 1b. Figure 1c shows the corresponding plot for photons measured in TE with $|\cos\theta| > 0.82$. The three events outside the accepted region of ±30 ns are rejected as cosmic rays. Figure 2a shows the distribution of the cluster shape variable S for events passing all selection criteria or failing only the cluster shape cut of the special background vetoes. Rejecting events with S greater than 0.2 preserves the $e^+e^- \to \nu\bar{\nu}\gamma(\gamma)$ Monte Carlo events, while in the data it removes very large clusters which have

8

been verified as being due to cosmic rays and beam related backgrounds. Figure 2b shows the effect of one of the directional forward veto cuts against its principal intended background, $e^+e^- \rightarrow e^+e^-\gamma$. This cut is designed to remove events in which a highly energetic particle travelling close to the beam direction balances most or all of the transverse momentum of the observed photon(s). The events plotted are those passing all cuts or failing only this cut. All the remaining $e^+e^- \rightarrow e^+e^-(\gamma)$ Monte Carlo background events fall into this cut region while the signal from the $e^+e^- \rightarrow \nu\overline{\nu}\gamma(\gamma)$ Monte Carlo has only a very small number there. The data distribution for this plot was checked and found to agree well with the Monte Carlo prediction.

3.2   Acoplanar-Photons Event Selection

The acoplanar-photons selection has two overlapping regions of kinematic acceptance in order to retain both sensitivity to low-energy photons and acceptance at large $|\cos\theta|$. These selections are based on analyses previously published by OPAL using data collected at centre-of-mass energies of 130-172 GeV [1]. Except where specified, cuts on photon candidates apply to the two highest energy photon candidates found within the kinematic acceptance. The event selection criteria are described below:

- **Kinematic acceptance.** Events are accepted as candidates if there are at least two electromagnetic clusters with scaled energy, x_γ, exceeding 0.05 in the polar angle region $15° < \theta < 165°$ ($|\cos\theta| < 0.966$). In order to retain sensitivity to physics processes producing low-energy photons, the minimum energy requirement is relaxed to 1.5 GeV deposited energy (corresponding to a photon energy of about 1.75 GeV [26]) for events with a photon candidate in the polar angle region $|\cos\theta| < 0.8$ provided this photon is associated to an in-time TOF hit as outlined below in the description of the timing requirements. These two selections are referred to below as the "high-energy" and "low-energy" selections, respectively. Background vetoes are applied differently for the two parts of the selection, as described below. The system consisting of the two highest energy photons must satisfy $p_T^{\gamma\gamma}/E_{\text{beam}} > 0.05$.

- **Photon conversion consistency requirements or charged track veto.** For the high-energy selection, events having tracking information consistent with the presence of at least one charged particle originating from the interaction point are rejected. The rejection criteria are designed to retain acceptance for events in which one or both of the photons convert. Hit information from each of CJ, CV, and SI (for $|\cos\theta| < 0.9$) are used to form independent estimators for the existence of charged particle activity. Events are rejected on the basis of azimuthal association of charged particle activity with the photon candidate clusters. To reject $e^+e^- \rightarrow \ell^+\ell^-\gamma\gamma$, an additional veto requires that there be no reconstructed charged track with transverse momentum exceeding 1 GeV, with associated hits in CV, and separated from each of the photon candidates by more than $15°$.

  The low-energy part of the selection does not allow photon conversions in the tracking chambers. It requires that there be no reconstructed charged track in the event with 20 or more hits in CJ.

- **Cluster quality.** Photon candidates within the polar angle region $|\cos\theta| < 0.75$ are required to have an angular cluster extent less than 250 mrad in both θ and ϕ. Additionally, to reduce background from cosmic rays which graze the electromagnetic calorimeter producing extended energy deposits that can be split by the clustering algorithm, photon candidates are required to be separated by at least $2.5°$ in azimuth. Events are rejected if a photon candidate cluster energy exceeds the beam energy by more than three standard deviations.

- **Forward energy vetoes.** The forward vetoes described for the single-photon selection are applied with the same thresholds.

9

- **Muon veto.** To suppress backgrounds arising from cosmic ray muon interactions or beam halo muons which can deposit significant energy in the calorimeter, the events must pass the muon veto described for the single-photon selection. Additionally, the first three individual vetoes of the special background vetoes described for the single-photon selection are applied to events in which no TOF information is present.

- **Timing requirements.** For the low-energy part of the selection, in order to ensure that the trigger is fully efficient for low-energy photons, we require that there be a photon in the barrel region with an associated in-time TOF hit. For the high-energy selection the event must have an associated in-time TOF or an associated in-time TE hit for at least one of the photon candidates. Events with a photon having an associated out-of-time TOF hit are rejected. Events in which one photon candidate has an associated out-of-time TE hit are retained provided they pass the other timing requirements. Finally, if there is a charged track associated with a cluster within the polar angle region $|\cos\theta| < 0.82$, the requirement of an associated in-time TOF hit is applied.

- **Selective multi-photon veto.** As for the single-photon selection, this veto is designed to reject backgrounds primarily from $e^+e^- \to \gamma\gamma(\gamma)$ whilst retaining acceptance for events with two or more photons and missing energy. Events are rejected if any of the following criteria are satisfied:

  - The total visible ECAL energy of the event exceeds $0.95\sqrt{s}$.
  - The acoplanarity angle of the two highest energy clusters is less than $2.5°$.
  - The missing momentum vector calculated from the two highest energy photon candidates satisfies $|\cos\theta_{\mathrm{miss}}| > 0.95$.
  - Events having three or more photon candidates (with deposited energy greater than 300 MeV) are rejected unless the system formed by the three highest energy photons is significantly aplanar (sum of the three opening angles $< 350°$) and the transverse momentum of the three-photon system exceeds $0.1E_{\mathrm{beam}}$. For events with an energy sum greater than 1 GeV in either end of FD or SW, the aplanarity cut is applied, using the forward detector as the third photon candidate.

The acoplanar-photons selection described above has a lower energy threshold for the most energetic photon than the single-photon selection. However the single-photon selection has more acceptance for events without time-of-flight information for the photons. In order to obtain the best overall acceptance for acoplanar-photons, we have added to the above described acoplanar-photons selection that part of the single-photon selection which is within the kinematic acceptance of the acoplanar-photons selection. This addition results in a relative increase in efficiency of 9% for Standard Model $e^+e^- \to \nu\bar{\nu}\gamma\gamma(\gamma)$ events.

4 Results

The results of the single-photon and acoplanar-photons selections are given below in sections 4.1 and 4.2. The measured cross-sections for each search topology are given and compared with Standard Model expectations. As no evidence for new physics processes is seen, the results are presented in terms of upper limits on $\sigma(e^+e^- \to XY) \cdot \mathrm{BR}(X \to Y\gamma)$ and $\sigma(e^+e^- \to XX) \cdot \mathrm{BR}^2(X \to Y\gamma)$. This is done both for the general case of massive X and Y, applicable to conventional supersymmetric models in which $X = \tilde{\chi}_2^0$ and $Y = \tilde{\chi}_1^0$, and also separately for the special case of $M_Y \approx 0$, which applies both to single and pair production of neutralinos in supersymmetric models in which the LSP is a light

gravitino and to single and pair production of excited neutrinos. All efficiencies are evaluated with the decay length of X set to zero.

For the purposes of new physics searches, only the $\sqrt{s} = 183$ GeV data are considered; the $\sqrt{s} = 130$ and 136 GeV data do not open any new kinematic regions, nor is the integrated luminosity at these energies sufficient to significantly improve the potential for discovery. For both the XX and XY searches, Monte Carlo samples were generated for a variety of mass points in the kinematically accessible region of the (M_X, M_Y) plane. To set limits for arbitrary M_X and M_Y, the efficiency over the entire (M_X, M_Y) plane is parametrized using the efficiencies calculated at the generated mass points. In the single-photon search topology, the regions with $M_X + M_Y < M_Z$ are kinematically accessible at $\sqrt{s} \approx M_Z$, and strong limits have already been reported [27]. In the acoplanar-photons search topology, limits have been reported for masses $M_X < M_Z/2$ [28]. In these low mass regions, possible radiative return to the Z^0 followed by $Z^0 \rightarrow XY$ or XX would yield very different event kinematics than those produced by the signal Monte Carlo generator. For these reasons, the search for XY production is restricted to the region with $M_X + M_Y > M_Z$, and the search for XX production is restricted to M_X values larger than about $M_Z/2$.

4.1 Single-Photon

After applying the selection criteria of the single-photon selection to the $\sqrt{s} = 130$, 136 and 183 GeV data samples, a total of 21, 39 and 191 events are selected. The expected contributions from cosmic ray and beam related backgrounds are 0.02, 0.02 and 0.4 events, respectively. These backgrounds have been estimated from events having out-of-time TOF or TE information but passing all other selection criteria and from events selected with looser criteria that have been visually scanned. Of the expected physics backgrounds from plausible sources, only $e^+e^- \rightarrow \gamma\gamma(\gamma)$, $e^+e^- \rightarrow \ell^+\ell^-\nu\bar{\nu}(\gamma)$, $e^+e^- \rightarrow \mu^+\mu^-\gamma$ and $e^+e^- \rightarrow \tau^+\tau^-\gamma$ have non-negligible contributions. Coming primarily from the $e^+e^- \rightarrow \ell^+\ell^-\nu\bar{\nu}(\gamma)$ and $\mu^+\mu^-\gamma$ final states, the total physics backgrounds contribute 0.07, 0.09 and 0.4 events, respectively, to the 130, 136 and 183 GeV samples. The background contributions are summarized in Table 1. For each of the three centre-of-mass energies, Table 2 shows the number of events observed, the number of events expected from the Standard Model process $e^+e^- \rightarrow \nu\bar{\nu}\gamma(\gamma)$ evaluated using the KORALZ generator and the sum of background events expected from other Standard Model physics processes with those from cosmic ray and beam related processes. The numbers of events observed agree with the numbers expected from $e^+e^- \rightarrow \nu\bar{\nu}\gamma(\gamma)$ plus the background. The estimated efficiencies for selecting $e^+e^- \rightarrow \nu\bar{\nu}\gamma(\gamma)$ events within the kinematic acceptance of the single-photon selection are also given in Table 2, as are the corresponding measured $e^+e^- \rightarrow \nu\bar{\nu}\gamma(\gamma)$ cross-sections within this kinematic acceptance, corrected for detector and selection efficiencies, and subtracting the estimated background. For both the single-photon and acoplanar-photons selections, efficiency losses due to vetoes on random detector occupancy range from about (2-4)% at the different centre-of-mass energies. Quoted efficiencies include these losses.

The total systematic error on the cross-section measurement is estimated to be 3.5%. The contributing uncertainties are from the integrated luminosity (0.5%), effects due to uncertainties on the electromagnetic calorimeter energy scale and resolution (0.7%) and the detector occupancy estimate (1%). In addition, the overall selection efficiency uncertainty (2%) is caused mainly by uncertainties in the simulation of the detector material and consequent photon conversion probabilities. An additional error of 2.5% is assigned based on the comparison of the estimated efficiency using two different event generators [1]. The cross-section as a function of centre-of-mass energy is plotted in Figure 3. In this plot the measured cross-sections for $\sqrt{s} = 130$ and 136 GeV are 11.1 ± 1.7 and 15.9 ± 1.9 pb, respectively. These are weighted averages of the 1995 data results with the results from this analysis.

The results for $\sqrt{s} = 161$ GeV and $\sqrt{s} = 172$ GeV are also plotted. The cross-section results from our earlier publication [1] have been corrected for the slightly different kinematic acceptance used in the analysis of those data. The corrected cross-sections, obtained for the 1995 and 1996 data at $\sqrt{s} = $ 130, 136, 161 and 172 GeV are 10.6 ± 2.4, 17.3 ± 3.0, 5.6 ± 0.8 and 5.8 ± 0.8 pb, respectively. For 1997 data at $\sqrt{s} = $ 130, 136 and 183 GeV the measured cross-sections are 11.6 ± 2.5, 14.9 ± 2.4 and 4.71 ± 0.34 pb, respectively. The curve shows the predicted cross-section from the KORALZ event generator for the Standard Model process $e^+e^- \rightarrow \nu\overline{\nu}\gamma(\gamma)$. The data are in reasonable agreement with the prediction.

In Figure 4a, the scaled energy of the most energetic photon is plotted against the cosine of its polar angle for events in the $\sqrt{s}$=183 GeV sample. The data are distributed as expected from the $e^+e^- \rightarrow \nu\overline{\nu}\gamma(\gamma)$ Monte Carlo. Similar agreement is found for the 130 and 136 GeV data. In Figure 4b the polar angle distribution for the $\sqrt{s}$=183 GeV sample is shown and agrees with the $e^+e^- \rightarrow \nu\overline{\nu}\gamma(\gamma)$ Monte Carlo expectation. If one calculates the recoil mass M_{recoil}, defined as the mass recoiling against the photon (or against the two-photon system), one expects a peak in the M_{recoil} distribution at M_{Z}, due to a large contribution from the decay $Z^0 \rightarrow \nu\overline{\nu}$. One clearly sees this feature in the data as shown in Figure 5. There is good agreement between data and Monte Carlo in this distribution for each of the three centre-of-mass energies.

The single-photon selection was designed to allow for the presence of a second photon in order to accept events from the $e^+e^- \rightarrow \nu\overline{\nu}\gamma\gamma$ process. In the $\sqrt{s} = $ 130, 136 and 183 GeV data sets, 2, 4 and 12 observed events are considered to be two-photon events (i.e. have a second photon with deposited energy exceeding 300 MeV in the ECAL). This is consistent with the expectations of 1.4, 1.7 and 11.3 events, respectively, from the KORALZ Monte Carlo.

4.1.1 Search for $e^+e^- \rightarrow XY$, $X \rightarrow Y\gamma$; General case: $M_Y \geq 0$

The single-photon selection described in Section 3 is designed to maximize acceptance for Standard Model $e^+e^- \rightarrow \nu\overline{\nu}\gamma(\gamma)$ events. However, when searching for signatures of the process $e^+e^- \rightarrow XY, X \rightarrow Y\gamma$, it is possible to implement further cuts to reduce the contribution from $e^+e^- \rightarrow \nu\overline{\nu}\gamma(\gamma)$, which is now considered as background. Depending on the values of M_X and M_Y, various combinations of the following cuts are applied to events in the single-photon sample:

- **Kinematic consistency:** The energy of the most energetic photon is required to lie within the range kinematically accessible to a photon from the process $e^+e^- \rightarrow XY$, $X \rightarrow Y\gamma$, after accounting for energy resolution effects.

- **Degraded resolution:** Events with $M_{\mathrm{recoil}} <$75 GeV are rejected if the most energetic photon lies in the region $0.72 < |\cos\theta| < 0.82$ or $|\cos\theta| > 0.945$. Energy resolution in these angular regions is known to be degraded.

- **Low recoil mass:** Require $M_{\mathrm{recoil}} <$75 GeV.

- **Z^0 radiative return:** The event is rejected if 75 GeV $< M_{\mathrm{recoil}} <$ 105 GeV.

The kinematic consistency cut and the degraded resolution cut are applied to all (M_X, M_Y) values. The low recoil mass cut is applied if $M_Y < 0.28 M_X - 18$ (GeV), in which case a significant portion of

the expected photon energy distribution is consistent with low recoil masses[5]. The radiative return cut is applied if the low recoil mass cut is not applied, and if M_X and M_Y are such that the difference between the maximum and minimum kinematically allowed photon energies (before energy resolution effects are considered) is greater than $0.3 E_{\text{beam}}$.

The selection efficiencies including the above cuts as a function of (M_X, M_Y) are given in Figure 6. Also illustrated is the region in which the radiative return cut is applied. In the region where $M_X - M_Y$ is small, photon energies are correspondingly small and efficiencies become low. Since uncertainties due to energy scale and resolution effects become significant in this region, we do not consider values of M_X and M_Y that lead to efficiencies of less than 40% in the absence of the recoil mass or radiative return cuts.

The number of selected events in the data consistent with each (M_X, M_Y) value is shown in Figure 7 and can be compared with the number expected from Standard Model $e^+e^- \to \nu\bar{\nu}\gamma(\gamma)$ events as shown in Figure 8. In general there is good agreement, and we proceed to set upper limits at 95% confidence level (CL) on the cross-section times branching ratio, $\sigma(e^+e^- \to XY) \cdot \text{BR}(X \to Y\gamma)$, which are shown in Figure 9. The upper limits are calculated taking into account the expected number of Standard Model $e^+e^- \to \nu\bar{\nu}\gamma(\gamma)$ background events estimated from KORALZ using the method described in [29]. Background from sources other than $e^+e^- \to \nu\bar{\nu}\gamma(\gamma)$, including the estimated cosmic ray and beam related background, is intentionally not taken into account in the limit calculations. The resulting upper limits range from 0.075 pb to 0.80 pb.

The systematic error on the efficiency for selecting events from potential new physics sources is due to the effects already discussed in section 4.1, as well as the uncertainty on the efficiency parametrization across the (M_X, M_Y) plane. The parametrization was compared to efficiencies obtained from the fully simulated Monte Carlo samples at 40 selected (M_X, M_Y) points, and a resulting systematic error of 1% (absolute) was assigned across the plane. The total relative systematic error varies from 2 to 6% depending on M_X, M_Y; its effect on the upper limits is small, and is calculated according to [30]. Uncertainties in the $\nu\bar{\nu}\gamma(\gamma)$ background estimate are also taken into account. Unlike the systematic error on the efficiency, a relatively small uncertainty in the background estimate can have a significant impact on the resulting 95% CL limit, especially when the number of expected events is large. To account for this uncertainty, a convolution is performed within the upper limit calculations. Contributing sources to the background uncertainty are: the factors considered in the cross-section measurement (3.5%), the estimated theoretical uncertainty in the $\nu\bar{\nu}\gamma(\gamma)$ cross-section (2%) based in part on a comparison between the KORALZ and NUNUGPV98 [31] event generators, and a contribution due to uncertainties in the energy scale. This last contribution is dependent on the values of M_X and M_Y; it is calculated separately at each (M_X, M_Y) point, and ranges from negligible to 5%.

4.1.2 Search for $e^+e^- \to XY$, $X \to Y\gamma$; Special case: $M_Y \approx 0$

The case $M_Y \approx 0$ is applicable to excited neutrino models and to some supersymmetric models mentioned earlier. The results presented above include this case and no separate analysis is performed, but the results are highlighted here. As described earlier, the 75 GeV recoil mass cut is applied for all M_X hypotheses, so that the expected number of events is small. For example, in the range $91 < M_X \lesssim 170$ GeV, the expected contribution from $\nu\bar{\nu}\gamma(\gamma)$ is 0.98 ± 0.12 events and there is one event observed. Although the numbers of expected and observed events are constant in this range, the

---

[5]This region was chosen so as to optimize the expected sensitivity. The optimization condition chosen was that the expected upper limit on $\sigma \cdot \text{BR}$ for new physics contributions be minimized, where the expected upper limit is defined as the average limit one would expect to set in the absence of new physics contributions. This definition has the advantage that it does not require one to specify the cross-section of possible new physics.

efficiency of the recoil mass cut increases with increasing values of M_X, leading to decreasing values for the resulting upper limits on $\sigma(e^+e^- \to XY) \cdot BR(X \to Y\gamma)$. For $M_X \gtrsim 170$ GeV, the kinematic consistency requirements become more restrictive than the recoil mass cut. There are no longer any events kinematically consistent with hypotheses of $M_X \gtrsim 173$ GeV; the background expectation in this region varies from 0.60 ± 0.11 events at 173 GeV to 0.04 ± 0.01 events at the kinematic limit. The resulting upper limits on $\sigma(e^+e^- \to XY) \cdot BR(X \to Y\gamma)$ for $M_Y \approx 0$ as a function of M_X range from 0.46 pb to 0.075 pb, as shown in Figure 10.

4.2 Acoplanar-Photons

The acoplanar-photons selection applied to the 130, 136 and 183 GeV data samples yields 2, 2 and 10 events, respectively, in good agreement with the KORALZ predictions of 1.02 ± 0.02, 1.22 ± 0.02 and 9.14 ± 0.09 events for the Standard Model $e^+e^- \to \nu\overline{\nu}\gamma\gamma(\gamma)$ contribution. The expected contributions from other Standard Model processes and from cosmic ray and beam related backgrounds are small: less than 0.05, 0.05 and 0.1 events, respectively. The numbers of events expected and observed at the three centre-of-mass energies are summarized in Table 3. Also shown are the selection efficiencies for $e^+e^- \to \nu\overline{\nu}\gamma\gamma(\gamma)$ events, within the kinematic acceptance of the selection, and the corresponding cross-section measurements at each centre-of-mass energy. The OPAL measurements of the cross-sections at $\sqrt{s} = 130$, 136, 161, 172 and 183 GeV are summarized in Table 4. The measurements at 130 and 136 GeV are weighted averages of the results obtained from the 1997 and 1995 data samples. The latter results, as well as the results at $\sqrt{s} = 161$ and 172 GeV, have been taken from our previous publication [1] and are corrected for the different definition of the kinematic acceptance.

Systematic errors arising from uncertainties on the electromagnetic calorimeter energy scale and resolution, the simulation of the detector material and consequent photon conversion probabilities, the integrated luminosity measurement and the detector occupancy estimate have been considered, and a relative systematic error of 8% is assigned to the cross-section measurements. This comes dominantly from uncertainty on the energy scale for low-energy photons and from comparison of different event generators [1].

The kinematic properties of the selected events in the combined 1997 data sample are displayed in Figures 11 and 12. They are compared with the predicted distributions for $e^+e^- \to \nu\overline{\nu}\gamma\gamma(\gamma)$ obtained using the KORALZ generator normalized to the integrated luminosity of the data. In each case plot (a) shows the recoil mass distribution of the selected acoplanar-photon pairs. These are peaked near the mass of the Z^0 as expected for contributions from $e^+e^- \to \nu\overline{\nu}\gamma\gamma(\gamma)$. The resolution of the recoil mass is typically 2-4 GeV for $M_{\mathrm{recoil}} \approx M_Z$. Plot (b) shows the distribution of the scaled energy of the least-energetic photon. Plot (c) shows the $\gamma\gamma$ invariant mass distribution for which the mass resolution is typically 0.6-1.4 GeV. Plot (d) shows the distribution in scaled transverse momentum of the selected two-photon system. The measured kinematic properties of the events are given in Table 5. There were no selected events with three photons, compared to an expectation from KORALZ of 0.52 ± 0.02 events.

In data taken in 1995 at $\sqrt{s} = 130$ and 136 GeV, we observed 8 events compared to 1.6 ± 0.1 expected from KORALZ [1]. However, the kinematic properties of these events, in particular the recoil mass distribution, agreed reasonably well with expectations. It was demonstrated that plausible detector or beam related backgrounds do not contribute to this excess. Analysis of the 1996 OPAL data samples taken at $\sqrt{s} = 161$ and 172 GeV selected a number of events which was consistent with the expected Standard Model background contributions. In the data taken in 1997 at $\sqrt{s} = 130$ and 136 GeV, we select a total of 4 events where 2.24 ± 0.03 are expected. The 1997 data are therefore consistent with the KORALZ expectation. However, the OPAL data samples at $\sqrt{s} = 130$ and 136 GeV continue to favour an excess of events over the expectation from KORALZ. Results on

this topology have also been reported by the ALEPH collaboration based on the analysis of 5.8 pb^{-1} of data taken at $\sqrt{s}$ = 130 and 136 GeV in 1995. That analysis has a kinematic acceptance similar to the one used by OPAL. No events were observed compared to a Monte Carlo expectation of two events [32].

As discussed in our previous publication, the status of event generators and analytical calculations of the Standard Model process $e^+e^- \rightarrow \nu\bar{\nu}\gamma\gamma(\gamma)$ is not yet satisfactory. We anticipate that on-going theoretical work by several authors will result in increased understanding of the actual precision of current approaches, and lead to improved approaches. In particular, a new and more complete calculation has recently appeared [31]. For now, however, with contributions from higher order processes not demonstrably under control, we do not know what theoretical uncertainty to assign to the KORALZ prediction.

In conclusion, the observed data excess over the KORALZ prediction at $\sqrt{s}$ = 130 and 136 GeV has not been resolved satisfactorily. Analysis of all data collected at these centre-of-mass energies by the other LEP experiments could help to resolve whether the observed effect is real, rather than simply a statistical fluctuation or a deficiency in the calculation of the Standard Model prediction.

In the data taken at $\sqrt{s}$ = 183 GeV, the agreement with expectations from KORALZ is rather good. The only point of note is the selection of two events with a rather high invariant mass for the $\gamma\gamma$ pair. As seen in Figure 12c these events populate the high-mass tail of the distribution expected from $e^+e^- \rightarrow \nu\bar{\nu}\gamma\gamma(\gamma)$. These events are both characterized by almost back-to-back photons in the polar angle region above $|\cos\theta| > 0.9$.

4.2.1 Search for $e^+e^- \rightarrow XX$, $X \rightarrow Y\gamma$; General case: $M_Y \geq 0$

Selected events are classified as consistent with a given value of M_X and M_Y if the energy of each of the photons falls within the region kinematically accessible to photons from the process $e^+e^- \rightarrow XX$, $X \rightarrow Y\gamma$, including resolution effects. The selection efficiencies at each generated grid point for the $e^+e^- \rightarrow XX$, $X \rightarrow Y\gamma$ Monte Carlo events at $\sqrt{s}$ = 183 GeV are shown in Table 6. These values include the efficiency of the kinematic consistency requirement which is higher than 95% at each generated point in the (M_X, M_Y) plane.

Figure 13 shows the 95% CL exclusion regions for $\sigma(e^+e^- \rightarrow XX) \cdot BR^2(X \rightarrow Y\gamma)$. The limits vary from 0.08 pb to 0.37 pb for $M_X > 45$ GeV and $M_X - M_Y > 5$ GeV. In the region 2.5 GeV $\leq M_X - M_Y < 5.0$ GeV, the efficiency falls off rapidly (see Table 6). However, even accounting for increased uncertainty on the efficiency, the limits in that region are better than about 1 pb for all (M_X, M_Y). Because of the uncertainties in the modelling of the Standard Model background, as discussed earlier and in [1], these limits and the limits presented below for this topology have been calculated without taking into account the background estimate. Events from $e^+e^- \rightarrow \nu\bar{\nu}\gamma\gamma(\gamma)$ are typically characterized by a high-energy photon from the radiative return to the Z^0 and a second lower energy photon. The kinematic consistency requirement is such that the two photons must have energies within the same (kinematically accessible) region. As M_X and M_Y increase, the allowed range of energy for the photons narrows and fewer $\nu\bar{\nu}\gamma\gamma(\gamma)$ events will be accepted. For the 10 selected events at $\sqrt{s}$ = 183 GeV, the distribution of the number of events consistent with a given mass point (M_X, M_Y) is consistent with the expectation from $e^+e^- \rightarrow \nu\bar{\nu}\gamma\gamma(\gamma)$ Monte Carlo.

Systematic errors are due primarily to limited Monte Carlo statistics at the generated (M_X, M_Y) points and the uncertainty on the efficiency parametrization across the (M_X, M_Y) plane. The combined relative uncertainty on the efficiency varies from about (3-6)% across the plane (for $M_X - M_Y > 5$

GeV). All systematic uncertainties are accounted for in the manner advocated in reference [30]. This also applies to the limits for the $M_Y \approx 0$ case, presented in the next section.

4.2.2 Search for $e^+e^- \rightarrow XX$, $X \rightarrow Y\gamma$; Special case: $M_Y \approx 0$

For the special case of $M_Y \approx 0$ the kinematic consistency requirements differ from those used for the general case. One can calculate [10] the maximum mass, $M_X^{\max}$, which is consistent with the measured three-momenta of the two photons, assuming a massless Y. A cut on $M_X^{\max}$ provides further suppression of the $\nu\bar{\nu}\gamma\gamma(\gamma)$ background while retaining high efficiency for the signal hypothesis. This is discussed in more detail in reference [1]. We require that the maximum kinematically allowed mass be greater than $M_X - 5$ GeV, which retains $97 \pm 2\%$ relative efficiency for signal at all values of M_X while suppressing much of the remaining $\nu\bar{\nu}\gamma\gamma(\gamma)$ background. Figure 14a shows the expected $M_X^{\max}$ distribution for signal Monte Carlo events with $M_X = 80$ GeV and for $e^+e^- \rightarrow \nu\bar{\nu}\gamma\gamma(\gamma)$ Monte Carlo events. Also shown is the distribution of the selected data events. In addition, we require that the recoil mass be less than 80 GeV, which approximately maximizes the expected sensitivity of the analysis for all M_X. This cut retains more than 50% of the signal efficiency, for all values of M_X, and dramatically reduces the residual $\nu\bar{\nu}\gamma\gamma(\gamma)$ background. This is most true in the region of low M_X and remains valid up to the kinematic limit. A recoil mass cut is not applied in the massive Y case since this would lead to a large loss of efficiency in certain regions of the (M_X, M_Y) plane. For the $M_Y \approx 0$ case, the efficiencies calculated from Monte Carlo events generated at 183 GeV are shown in Table 7 after application of the event selection criteria and the cut on $M_X^{\max}$, and then after the additional requirement of $M_{\mathrm{recoil}} < 80$ GeV. Also shown in Figure 14 are the M_{recoil} distributions for selected events with (b) no cut on $M_X^{\max}$ and (c) $M_X^{\max} > 75$ GeV (for consistency with $M_X = 80$ GeV). No event survives the recoil mass cut; the expected number of Standard Model events is 0.66 ± 0.03. The expected number consistent with $M_X \geq 45$ GeV is 0.36 ± 0.02 decreasing to 0.07 ± 0.01 expected events consistent with $M_X \geq 90$ GeV as shown in Table 7.

Based on the efficiencies and the number of selected events, we calculate a 95% CL upper limit on $\sigma(e^+e^- \rightarrow XX) \cdot \mathrm{BR}^2(X \rightarrow Y\gamma)$ for $M_Y \approx 0$ as a function of M_X. This is shown as the solid line in Figure 15. The limit ranges from 0.094 to 0.14 pb for all M_X from 45 GeV to the kinematic limit. Also shown as a dashed line is the expected limit, defined in section 4.1.1. These limits can be used to set model-dependent limits on the mass of the lightest neutralino in supersymmetric models in which the NLSP is the lightest neutralino and the LSP is a light gravitino ($X = \tilde{\chi}_1^0, Y = \tilde{G}$). Shown in Figure 15 as a dotted line is the (Born-level) cross-section prediction from a specific light gravitino LSP model [12] in which $M(\tilde{e}_R) = 1.35M(\tilde{\chi}_1^0)$, $M(\tilde{e}_L) = 2M(\tilde{e}_R)$ and the neutralino composition is purely gaugino (bino). Within the framework of this model, $\tilde{\chi}_1^0$ masses between 45 and 83 GeV are excluded at 95% CL. The expected number of $\nu\bar{\nu}\gamma\gamma(\gamma)$ background events consistent with $M_X \geq 83$ GeV is 0.12 ± 0.01.

As described in section 2, the efficiencies over the full angular range have been calculated using isotropic angular distributions for production and decay of X. The validity of this model has been examined based on the angular distributions calculated for photino pair production in [8]. For models proposed in [9], the production angular distributions are more central and so this procedure is conservative. For a $1 + \cos^2\theta$ production angular distribution expected for t-channel exchange of a very heavy particle according to [8], the relative efficiency reduction would be less than 2% at all points in the (M_X, M_Y) plane.

5   Conclusions

We have searched for photonic events with large missing energy in two topologies in data taken with the OPAL detector at LEP, at centre-of-mass energies of 130, 136 and 183 GeV.

In the single-photon selection, which requires at least one photon with $x_T > 0.05$ in the region $15° < \theta < 165°$ ($|\cos\theta| < 0.966$), a total of 21, 39 and 191 events are observed in the data for $\sqrt{s} = 130$, 136 and 183 GeV, respectively. These numbers are in agreement with the expectations of the KORALZ Monte Carlo generator for the Standard Model process $e^+e^- \rightarrow \nu\bar{\nu}\gamma(\gamma)$. The expected background is small. We derive upper limits on the cross-section times branching ratio for the process $e^+e^- \rightarrow XY$, $X \rightarrow Y\gamma$ for the general case of massive X and Y. The limits vary from 0.075 to 0.80 pb in the region of interest in the (M_X, M_Y) plane and include the special case of $M_Y \approx 0$, where the limit varies between 0.075 and 0.46 pb for the M_X mass range from M_Z to 183 GeV.

The acoplanar-photons selection requires at least two photons with scaled energy $x_\gamma > 0.05$ within the polar angle region $15° < \theta < 165°$ or at least two photons with energy $E_\gamma > 1.75$ GeV with one satisfying $|\cos\theta| < 0.8$ and the other satisfying $15° < \theta < 165°$. In each case, the requirement $p_T^{\gamma\gamma}/E_{\text{beam}} > 0.05$ is also applied. A total of 2, 2 and 10 events are selected from the data samples at $\sqrt{s} = 130$, 136 and 183 GeV, respectively. The KORALZ predictions for the contributions from $e^+e^- \rightarrow \nu\bar{\nu}\gamma\gamma(\gamma)$ are, respectively, 1.02, 1.22 and 9.14 events. The number of events observed in the 1997 data samples and their kinematic distributions are consistent with expectations for $e^+e^- \rightarrow \nu\bar{\nu}\gamma\gamma(\gamma)$. We derive 95% CL upper limits on $\sigma(e^+e^- \rightarrow XX) \cdot BR^2(X \rightarrow Y\gamma)$ ranging from 0.08 to 0.37 pb for the general case of massive X and Y. For the special case of $M_Y \approx 0$, the 95% CL upper limits on $\sigma(e^+e^- \rightarrow XX) \cdot BR^2(X \rightarrow Y\gamma)$ range from 0.094 to 0.14 pb. Due to the uncertainties in the current modelling of the Standard Model process $e^+e^- \rightarrow \nu\bar{\nu}\gamma\gamma(\gamma)$, all limits from the acoplanar-photons analysis were calculated without taking into account the background estimate.

For the single-photon and acoplanar-photons search topologies, the general case of massive X and Y is relevant to supersymmetric models in which $X = \tilde{\chi}_2^0$ and $Y = \tilde{\chi}_1^0$, with $\tilde{\chi}_2^0 \rightarrow \tilde{\chi}_1^0\gamma$ and $\tilde{\chi}_1^0$ stable. The special case of $M_Y \approx 0$ is of particular interest for single and pair production of excited neutrinos and for supersymmetric models in which the LSP is a light gravitino and the NLSP is $\tilde{\chi}_1^0$ which decays as $\tilde{\chi}_1^0 \rightarrow \tilde{G}\gamma$. For the latter scenario, the results of the acoplanar-photons search are used to place model-dependent lower limits on the $\tilde{\chi}_1^0$ mass. A specific light gravitino LSP model [12] is excluded for the case of promptly decaying neutralinos with masses between 45 and 83 GeV.

6   Acknowledgements

References

[1] OPAL Collab., K. Ackerstaff et al., Eur. Phys. J. **C2** (1998) 607.

[2] OPAL Collab., K. Ackerstaff et al., CERN-EP/98-092, submitted to Eur. Phys. J. **C**.

[3] ALEPH Collab., R. Barate et al., Phys. Lett. **B420** (1998)127;
DELPHI Collab., P. Abreu et al., Eur. Phys. J. **C1** (1998) 1;
L3 Collab., M. Acciarri et al., Phys. Lett. **B415** (1997) 299.

[4] ALEPH Collab., R. Barate et al., Phys. Lett. **B429** (1998) 201.

[5] D0 Collab., S. Abachi et al., Phys. Rev. Lett. **78** (1997) 2070;
CDF Collab., F. Abe et al., hep-ex/9806034, submitted to Phys. Rev. **D**.

[6] S. Ambrosanio et al., Phys. Rev. Lett. **76** (1996) 3498; Phys. Rev. **D55** (1997) 1392.

[7] H. Komatsu and J. Kubo, Phys. Lett. **B157** (1985) 90; Phys. Lett. **B162** (1985) 379;
H.E. Haber and D. Wyler, Nucl. Phys. **B323** (1989) 267;
S. Ambrosanio and B. Mele, Phys. Rev. **D53** (1996) 2541.

[8] J. Ellis and J.S. Hagelin, Phys. Lett. **B122** (1983) 303.

[9] S. Dimopoulos et al., Phys. Rev. Lett. **76** (1996) 3494;
D.R. Stump, M. Wiest, C.P. Yuan, Phys. Rev. **D54** (1996) 1936;
S. Ambrosanio et al., Phys. Rev. **D54** (1996) 5395.

[10] J.L. Lopez and D.V. Nanopoulos, Mod. Phys. Lett. **A11** (1996) 2473;
Phys. Rev. **D55** (1997) 4450.

[11] J.L. Lopez, D.V. Nanopoulos and A. Zichichi, Phys. Rev. Lett. **77** (1996) 5168.

[12] C.Y. Chang and G.A. Snow, UMD/PP/97-57.
K. S. Babu, C. Kolda and F. Wilczek, Phys. Rev. Lett. **77** (1996) 3070.

[13] A. Brignole, F. Feruglio and F. Zwirner, Nucl. Phys. **B516** (1998) 13.

[14] OPAL Collab, K. Ackerstaff et al., CERN-EP/98-093, submitted to Phys. Lett. **B**.

[15] OPAL Collab., K. Ackerstaff et al., Eur. Phys. J. **C1** (1998) 45;
OPAL Collab., G. Abbiendi et al, "Search for Chargino and Neutralino Production at $\sqrt{s} = $ 181-184 GeV at LEP", submitted to Eur. Phys. J. **C**.

[16] OPAL Collab., K. Ahmet et al., Nucl. Instrum. Methods **A305** (1991) 275;
S. Anderson et al., Nucl. Instrum. Methods **A403** (1998) 326;
B.E. Anderson et al., IEEE Transactions on Nuclear Science **41** (1994) 845.

[17] G. Aguillion et al., CERN-EP/98-069 (to be published in Nucl. Instrum. Methods).

[18] M. Arignon et al., Nucl. Instrum. Methods **A313** (1992) 103.

[19] S. Jadach, B.F.L. Ward and Z. Wąs, Comp. Phys. Comm. **79** (1994) 503.
Version 4.02 was used including a recommended correction to the NDIST0 subroutine.

[20] F.A. Berends and R. Kleiss, Nucl. Phys. **B186** (1981) 22.

[21] S. Jadach, W. Placzek and B.F.L. Ward, Phys. Lett. **B390** (1997) 298.

[22] D. Karlen, Nucl. Phys. **B289** (1987) 23.

[23] J. Fujimoto et al., Comp. Phys. Comm. **100** (1997) 128.

[24] S. Katsanevas and S. Melachronios, CERN/96-01, Vol.2 (1996) 328.

[25] J. Allison et al., Nucl. Instrum. Methods **A317** (1992) 47.

[26] OPAL Collab., R. Akers et al., Z. Phys. **C65** (1995) 47.

[27] L3 Collab., M. Acciarri et al., Phys. Lett. **B350** (1995) 109;
OPAL Collab., G. Alexander et al., Phys. Lett. **B377** (1996) 273.

[28] OPAL Collab., M.Z. Akrawy et al., Phys. Lett. **B248** (1990) 211;
ALEPH Collab., D. Decamp et al., Phys. Rep. **216** (1992) 253;
L3 Collab., M. Acciarri et al., Phys. Lett. **B350** (1995) 109.

[29] Particle Data Group, R.M. Barnett et al., Phys. Rev. **D54** (1996) 1.

[30] R.D. Cousins and V.L. Highland, Nucl. Instrum. Methods **A320** (1992) 331.

[31] G. Montagna, M. Moretti, O. Nicrosini and F. Piccinini, CERN-TH/98-238.

[32] ALEPH Collab., D. Buskulic et al., Phys. Lett. **B384** (1996) 333.

Background process	$\sqrt{s}$=130 GeV	$\sqrt{s}$=136 GeV	$\sqrt{s}$=183 GeV
$e^+e^- \to \mu^+\mu^-(\gamma)$	$.04 \pm .01$	$.05 \pm .01$	$.20 \pm .04$
$e^+e^- \to \ell^+\ell^-\nu\bar{\nu}(\gamma)$	$.02 \pm .01$	$.03 \pm .01$	$.12 \pm .03$
$e^+e^- \to \tau^+\tau^-(\gamma)$	$.01 \pm .01$	$.01 \pm .01$	$.03 \pm .01$
$e^+e^- \to \gamma\gamma(\gamma)$	$<.02$	$<.03$	$.03 \pm .02$
Total physics bkgd.	$.07 \pm .02$	$.09 \pm .02$	$.38 \pm .05$
Other bkgd.	$.02 \pm .02$	$.02 \pm .02$	$.39 \pm .14$
Total background	$.09 \pm .03$	$.11 \pm .03$	$.77 \pm .15$

Table 1: Numbers of events expected from various background processes contributing to the single-photon event sample for the three centre-of-mass energies. The Standard Model background contributions are given by process. Also shown are the expected other backgrounds coming from cosmic rays and beam related sources. The errors shown are statistical and the upper limits are at 68% CL.

$\sqrt{s}$(GeV)	N_{obs}	$N_{\nu\bar{\nu}\gamma(\gamma)}$	N_{bkg}	$\epsilon_{\nu\bar{\nu}\gamma(\gamma)}(\%)$	$\sigma_{meas}^{\nu\bar{\nu}\gamma(\gamma)}$(pb)
130	21	25.8 ± 0.1	0.09 ± 0.03	77.0 ± 0.4	11.6 ± 2.5
136	39	31.2 ± 0.2	0.11 ± 0.03	77.5 ± 0.4	14.9 ± 2.4
183	191	201.3 ± 0.7	0.77 ± 0.15	74.2 ± 0.3	4.71 ± 0.34

Table 2: For each centre-of-mass energy, the table shows the number of events from the single-photon selection observed in the 1997 OPAL data, the number expected based on the KORALZ $e^+e^- \to \nu\bar{\nu}\gamma(\gamma)$ event generator and the number of events expected from backgrounds. Also shown are the efficiencies for $e^+e^- \to \nu\bar{\nu}\gamma(\gamma)$ within the kinematic acceptance of the single-photon selection (defined in section 3) and the background-subtracted measured cross-sections within the kinematic acceptance. The errors shown are statistical.

$\sqrt{s}$(GeV)	N_{obs}	$N_{\nu\bar{\nu}\gamma\gamma(\gamma)}$	$\epsilon_{\nu\bar{\nu}\gamma\gamma(\gamma)}(\%)$	$\sigma_{meas}^{\nu\bar{\nu}\gamma\gamma(\gamma)}$(pb)
130	2	1.02 ± 0.02	69.3 ± 1.0	1.23 ± 0.87
136	2	1.22 ± 0.02	69.1 ± 0.7	0.86 ± 0.61
183	10	9.14 ± 0.09	67.9 ± 0.4	0.27 ± 0.09

Table 3: For each centre-of-mass energy, the table shows the number of selected acoplanar-photons events in the 1997 OPAL data and the number expected based on the KORALZ $e^+e^- \to \nu\bar{\nu}\gamma\gamma(\gamma)$ event generator. Also shown are the efficiencies for $e^+e^- \to \nu\bar{\nu}\gamma\gamma(\gamma)$ events within the kinematic acceptance of the acoplanar-photons selection (defined in section 3) and the corresponding cross-section measurements.

$\sqrt{s}$(GeV)	$\sigma_{meas}^{\nu\bar{\nu}\gamma\gamma(\gamma)}$(pb)	$\sigma_{KORALZ}^{\nu\bar{\nu}\gamma\gamma(\gamma)}$(pb)
130	1.49 ± 0.68	0.626 ± 0.010
136	1.23 ± 0.56	0.526 ± 0.008
161	0.16 ± 0.16	0.330 ± 0.018
172	0.32 ± 0.23	0.303 ± 0.017
183	0.27 ± 0.09	0.247 ± 0.002

Table 4: The measured cross-section for the process $e^+e^- \to \nu\bar{\nu}\gamma\gamma(\gamma)$, within the kinematic acceptance defined in section 3, for different centre-of-mass energies. For $\sqrt{s} = 130$ and 136 GeV the measurements are the weighted average of the results obtained from the 1997 data and the results obtained from the 1995 data. The latter results, as well as those at $\sqrt{s} = 161$ and 172 GeV, are taken from our previous publication [1] and have been corrected for the different definition of the kinematic acceptance. The final column shows the cross-section predictions from KORALZ. The quoted errors are statistical.

$\sqrt{s}$	x_1	x_2	$\cos\theta_1$	$\cos\theta_2$	ϕ_1	ϕ_2	M_{recoil}	$M_{\text{X}}^{\text{max}}$	$M_{\gamma\gamma}$	$p_T^{\gamma\gamma}/E_{\text{beam}}$
130.0	0.175	0.059	0.266	0.264	5.637	5.006	113.8	29.8	4.0	0.218
130.0	0.263	0.266	0.296	0.956	3.574	2.162	91.4	54.3	20.0	0.275
135.9	0.432	0.063	-0.801	0.928	3.037	5.901	99.1	7.3	22.2	0.236
136.0	0.367	0.234	0.482	0.657	2.372	0.847	88.9	57.2	22.7	0.373
182.8	0.484	0.221	-0.958	0.125	2.138	1.318	107.4	74.6	40.6	0.329
182.7	0.674	0.061	0.867	0.451	4.367	4.788	94.7	43.2	11.8	0.387
182.7	0.519	0.518	0.957	-0.965	4.848	4.556	84.1	91.3	91.2	0.282
182.7	0.726	0.096	0.706	-0.737	5.076	2.587	90.3	16.4	47.1	0.464
182.7	0.761	0.026	0.293	-0.883	4.921	0.762	87.2	16.2	22.4	0.721
182.7	0.307	0.059	0.907	-0.728	2.103	2.558	146.9	33.8	20.6	0.166
182.7	0.604	0.028	0.913	-0.611	0.051	5.073	112.6	18.0	20.3	0.254
182.6	0.709	0.067	0.551	0.844	0.985	1.005	87.0	45.5	8.3	0.627
182.7	0.541	0.416	-0.915	0.901	1.490	6.115	91.4	82.7	83.1	0.271
182.7	0.541	0.156	-0.841	0.903	3.050	5.363	113.2	25.3	51.9	0.252

Table 5: Kinematic properties of selected acoplanar-photons events. Energies and masses are in GeV. Angles are in radians. The quantity $M_{\text{X}}^{\text{max}}$ is defined in section 4.2.2.

M_{X}	$M_{\text{Y}}=0$	$M_{\text{Y}} = M_{\text{X}}/2$	$M_{\text{Y}} = M_{\text{X}} - 10$	$M_{\text{Y}} = M_{\text{X}} - 5$	$M_{\text{Y}} = M_{\text{X}} - 2.5$
90	71.8 ± 1.3	71.0 ± 1.4	65.5 ± 1.4	39.2 ± 1.5	6.8 ± 0.8
85	72.5 ± 1.3	71.8 ± 1.3	64.4 ± 1.4	40.0 ± 1.5	7.6 ± 0.8
80	71.9 ± 1.3	71.2 ± 1.4	65.7 ± 1.4	41.4 ± 1.5	5.9 ± 0.7
70	71.5 ± 1.4	70.0 ± 1.4	63.9 ± 1.4	46.0 ± 1.5	6.6 ± 0.7
60	73.1 ± 1.3	74.2 ± 1.3	64.3 ± 1.4	43.5 ± 1.5	7.7 ± 0.8
50	73.7 ± 1.3	72.2 ± 1.3	64.3 ± 1.4	43.7 ± 1.5	9.4 ± 0.9

Table 6: Acoplanar-photons selection efficiencies (%) for the process $e^+e^- \to XX$, $X \to Y\gamma$ at $\sqrt{s} = 183$ GeV for various M_{X} and M_{Y} (in GeV). These values include the efficiency of the kinematic consistency cuts. The efficiencies for the generated points at $M_{\text{Y}} = 20$ and $M_{\text{Y}} = M_{\text{X}} - 15$ are not shown.

M_{X}	Selection efficiency with $M_{\text{X}}^{\text{max}} > M_{\text{X}} - 5$ GeV	Selection efficiency with $M_{\text{recoil}} < 80$ GeV	$N_{\nu\bar{\nu}\gamma\gamma(\gamma)}$
90	71.3 ± 1.4	57.5 ± 1.5	0.07 ± 0.01
85	71.6 ± 1.4	53.8 ± 1.5	0.10 ± 0.01
80	70.0 ± 1.4	47.1 ± 1.5	0.13 ± 0.01
70	69.2 ± 1.4	40.7 ± 1.5	0.18 ± 0.01
60	70.4 ± 1.4	42.7 ± 1.5	0.25 ± 0.02
50	70.4 ± 1.4	37.2 ± 1.5	0.31 ± 0.02

Table 7: Acoplanar-photons event selection efficiency (%), as a function of mass, for the process $e^+e^- \to XX$, $X \to Y\gamma$, for $M_{\text{Y}} \approx 0$ at $\sqrt{s} = 183$ GeV. The first column shows the efficiency of the selection described in section 3.2, after the cut on $M_{\text{X}}^{\text{max}}$. The second column shows the efficiency (%) after the additional requirement that $M_{\text{recoil}} < 80$ GeV. The last column shows the expected number of events from the process $e^+e^- \to \nu\bar{\nu}\gamma\gamma(\gamma)$ (KORALZ). The errors are statistical.
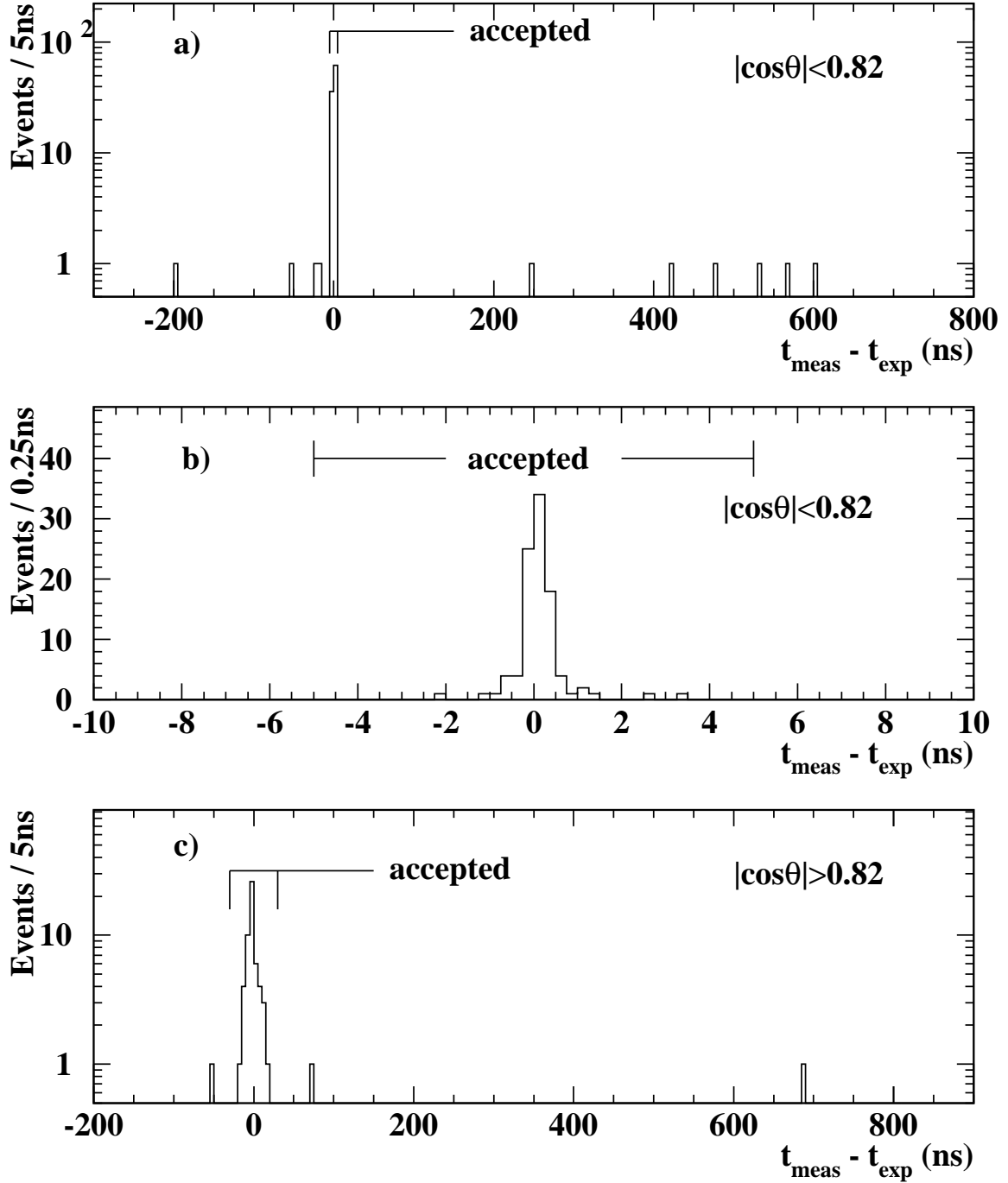
OPAL

Figure 1: For single-photon candidates in the data, a) shows the difference between the measured time-of-flight in the TOF and that expected for a photon from the interaction point for events passing all cuts or failing only the TOF timing cut; b) the same plot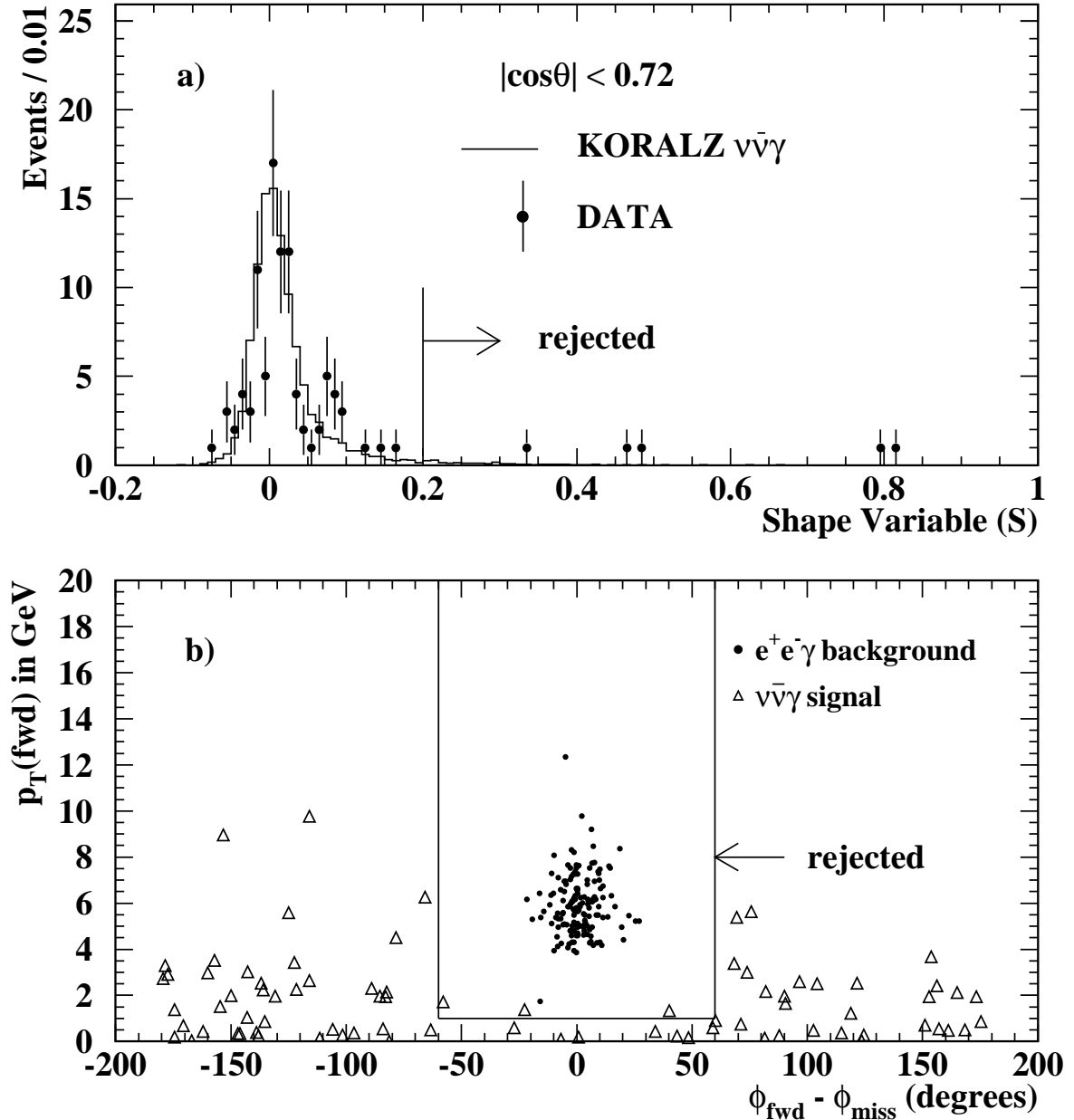 but magnifying the expected region for good events; c) shows the difference between the measured time-of-flight in the TE scintillators and that expected for a photon from the interaction point for events passing all cuts or failing only the TE timing cut.

OPAL

Figure 2: a) The distribution for the cluster shape variable S, for the KORALZ $e^+e^- \rightarrow \nu\bar{\nu}\gamma(\gamma)$ Monte Carlo (histogram) and for data (points). Events must have the primary photon candidate within $|\cos\theta| < 0.72$ and passing all cuts or failing only the special background vetoes. The Monte Carlo sample is normalized to the integrated luminosity of the data. b) The transverse momentum sum of hits measured in the FD and SW calorimeters is plotted against the difference in azimuth between the forward momentum sum and the direction opposite the measured photonic system. The events plotted are those passing all cuts or failing only this cut. The solid circles are from the $e^+e^- \rightarrow e^+e^-\gamma$ Monte Carlo while the open triangles are from the $e^+e^- \rightarrow \nu\bar{\nu}\gamma(\gamma)$ Monte Carlo. Most $e^+e^- \rightarrow \nu\bar{\nu}\gamma(\gamma)$ events have no significant forward energy and are not shown in the plot. The number of events correspond to ten times the integrated luminosity of the data.
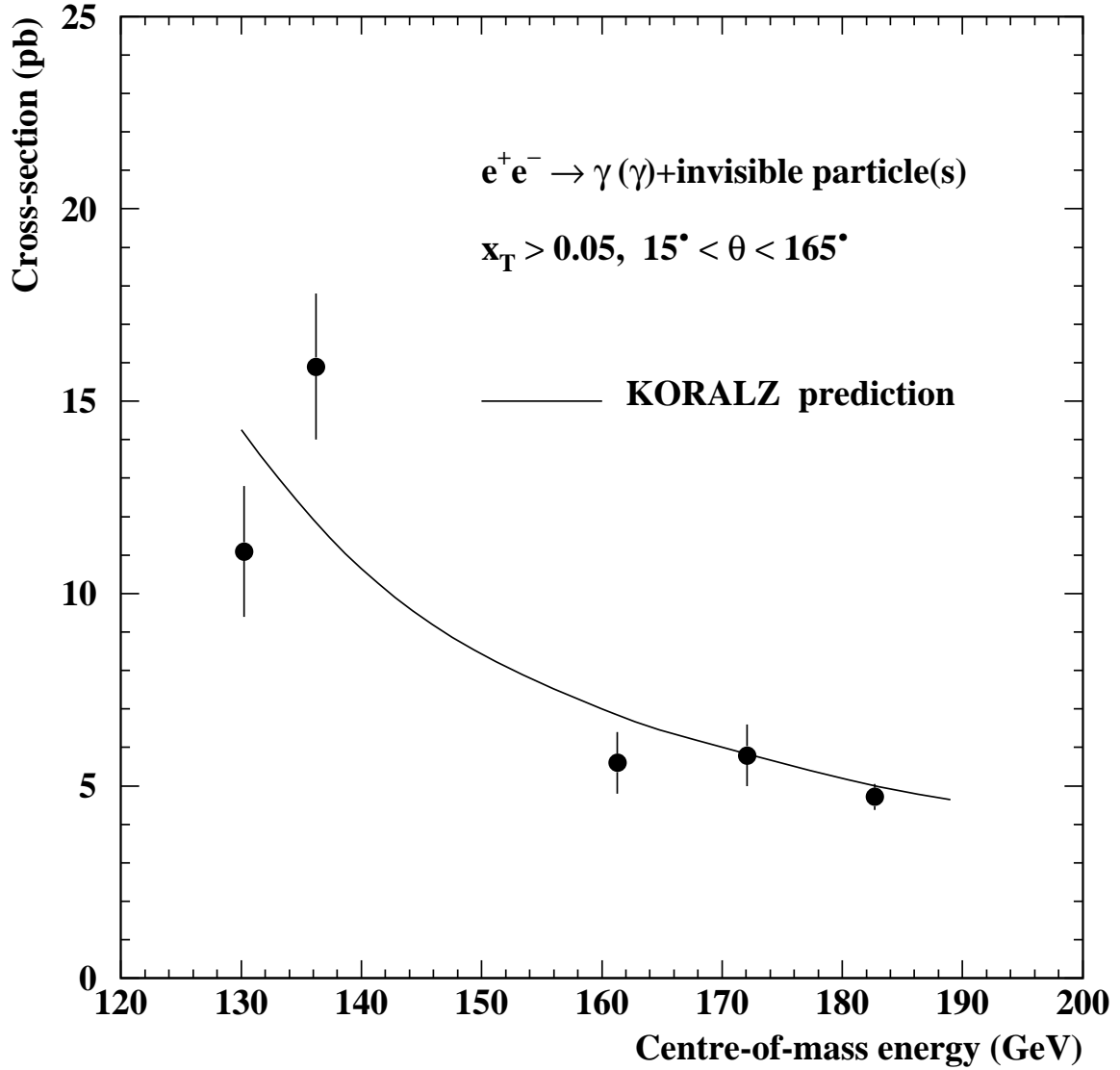
OPAL

Figure 3: The measured value of $\sigma(e^+e^- \rightarrow \gamma(\gamma) + $ invisible particle(s)), within the kinematic acceptance of the single-photon selection, as a function of $\sqrt{s}$. The data points with error bars are OPAL measurements at $\sqrt{s}$ = 130, 136, 161, 172 and 183 GeV. The curve is the prediction for the Standard Model process $e^+e^- \rightarrow \nu\bar{\nu}\gamma(\gamma)$ from the KORALZ generator. The data points at 130 and 136 GeV represent the weighted means of cross-section measurements obtained from the 1995 and 1997 data samples. The cross-section measurements from the previous data sets at $\sqrt{s}$ = 130, 136, 161 and 172 GeV have been corrected for the difference in kinematic acceptance from the present analysis.

24

OPAL
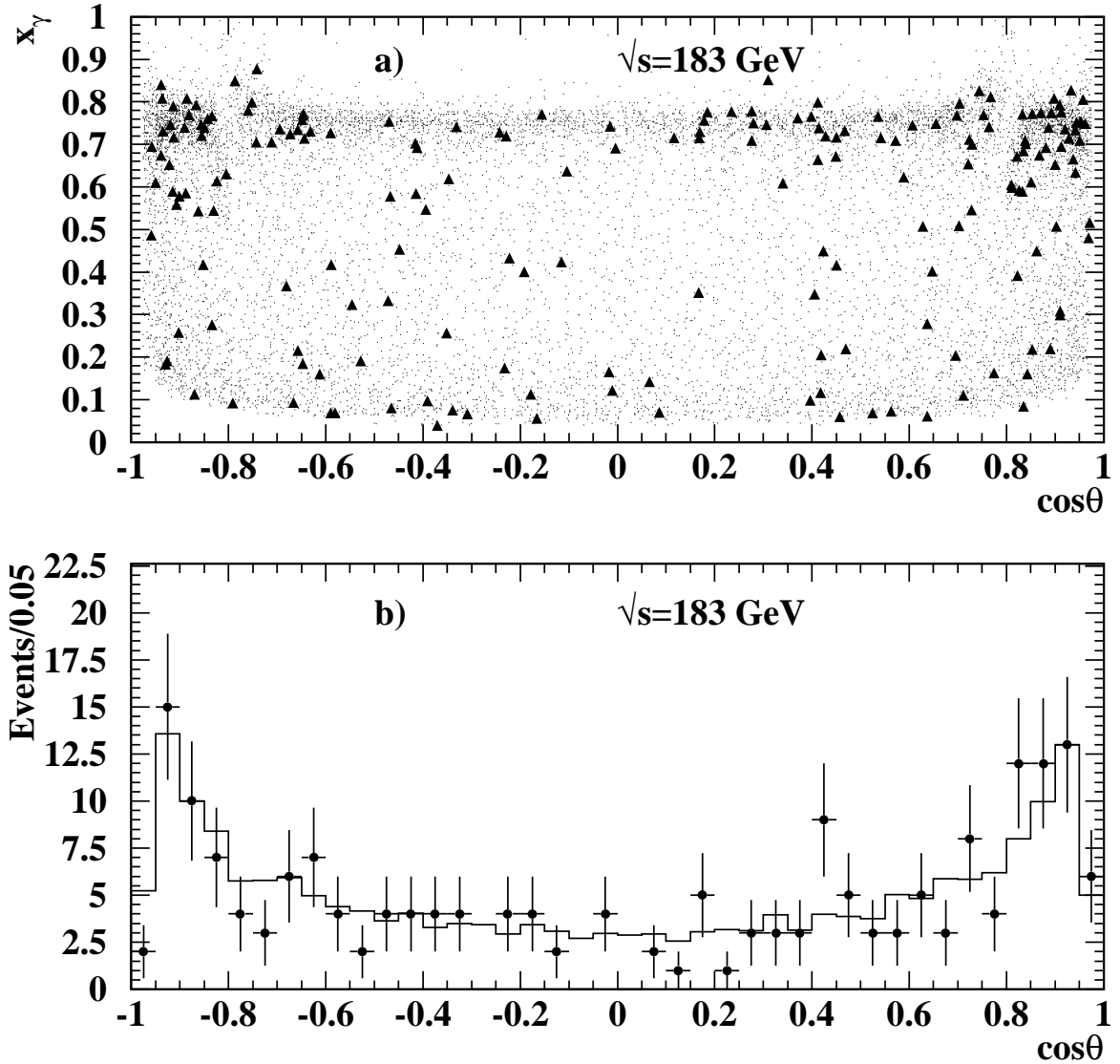
Figure 4: a) Distribution of x_γ vs $\cos\theta$ for the most energetic photon in the single-photon selection at $\sqrt{s} = 183$ GeV. The fine points are the KORALZ $e^+e^- \to \nu\bar{\nu}\gamma(\gamma)$ Monte Carlo (arbitrary normalization) and the solid triangles are the data. b) The $\cos\theta$ distribution for the most energetic photon in the single-photon selection at $\sqrt{s} = 183$ GeV. The points with error bars are the data and the histogram is the expectation from the KORALZ $e^+e^- \to \nu\bar{\nu}\gamma(\gamma)$ Monte Carlo normalized to the integrated luminosity of the data.

25
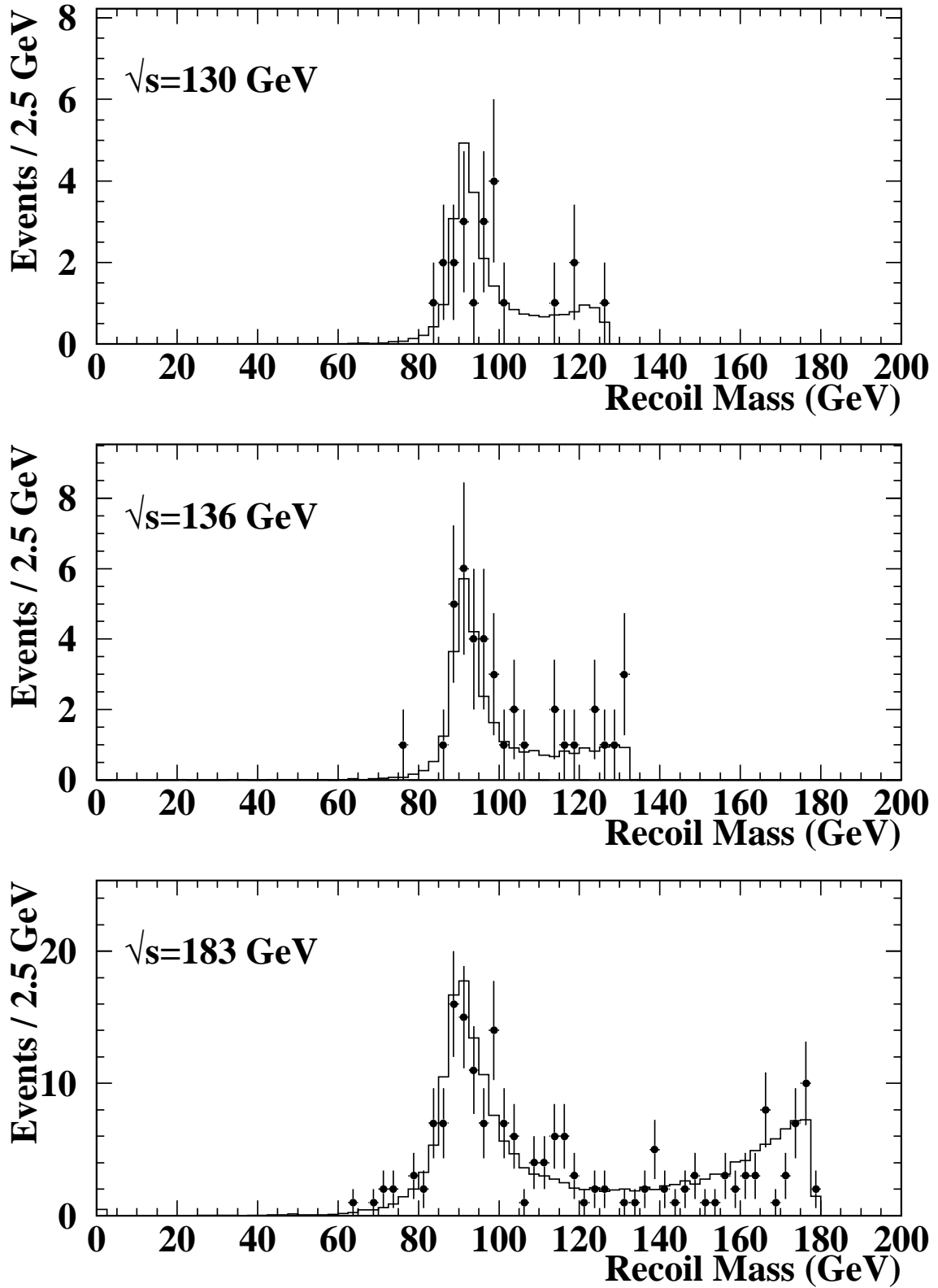
Figure 5: The recoil mass distribution for events passing the single-photon selection for the $\sqrt{s} = 130$, 136 and 183 GeV data samples. The points with error bars are the data and the histograms are the expectations from the KORALZ $e^+e^- \rightarrow \nu\overline{\nu}\gamma(\gamma)$ Monte Carlo normalized to the integrated luminosity of the data.

OPAL
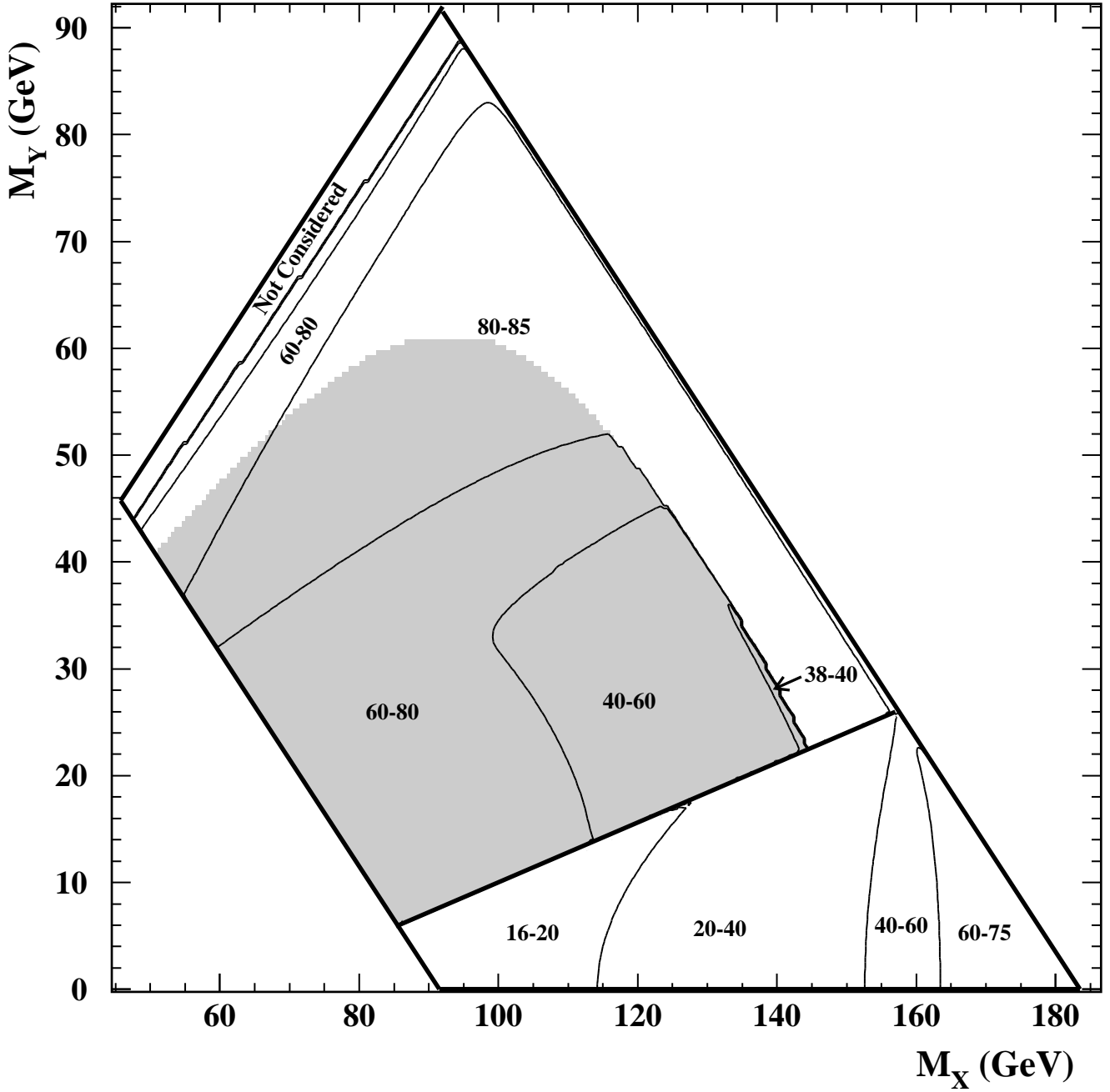
Figure 6: Single-photon selection efficiency contours (in %) for $\sqrt{s} = 183$ GeV as a function of M_X and M_Y. Lines are drawn around the boundaries defined by $M_X + M_Y = 183$ GeV, $M_X = M_Y$, and $M_X + M_Y = M_Z$, and to display the boundary between the small and large M_Y regions. The shaded region indicates where the radiative return cut is applied. The region in which $M_X - M_Y$ is small is not considered, as explained in the text.

OPAL
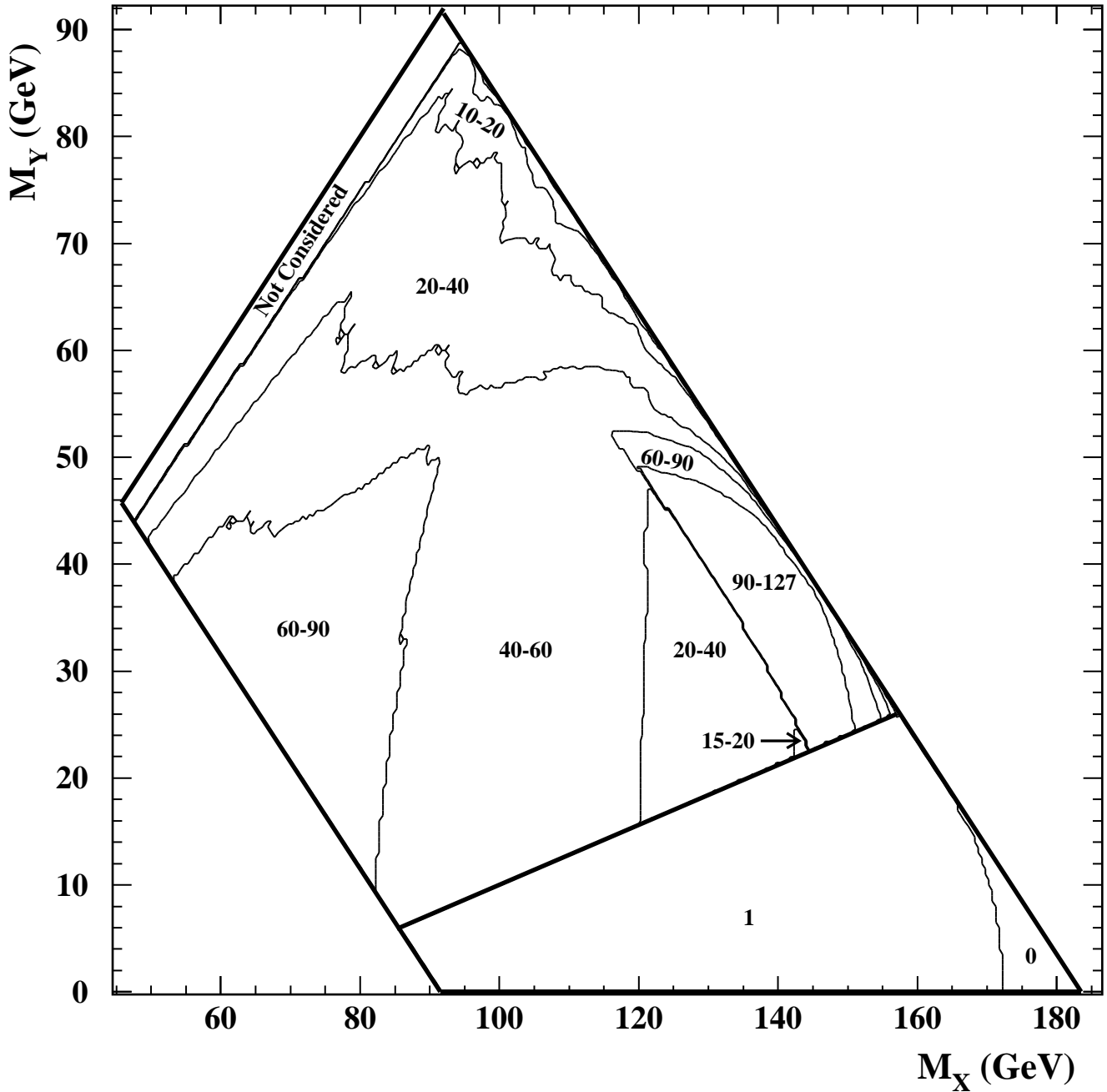
Figure 7: Number of single-photon candidate events in the $\sqrt{s} = 183$ GeV data sample consistent with each set of mass values (M_X, M_Y) for the process $e^+e^- \to XY$, $X \to Y\gamma$. The boundaries and delineated regions are as defined for Figure 6.
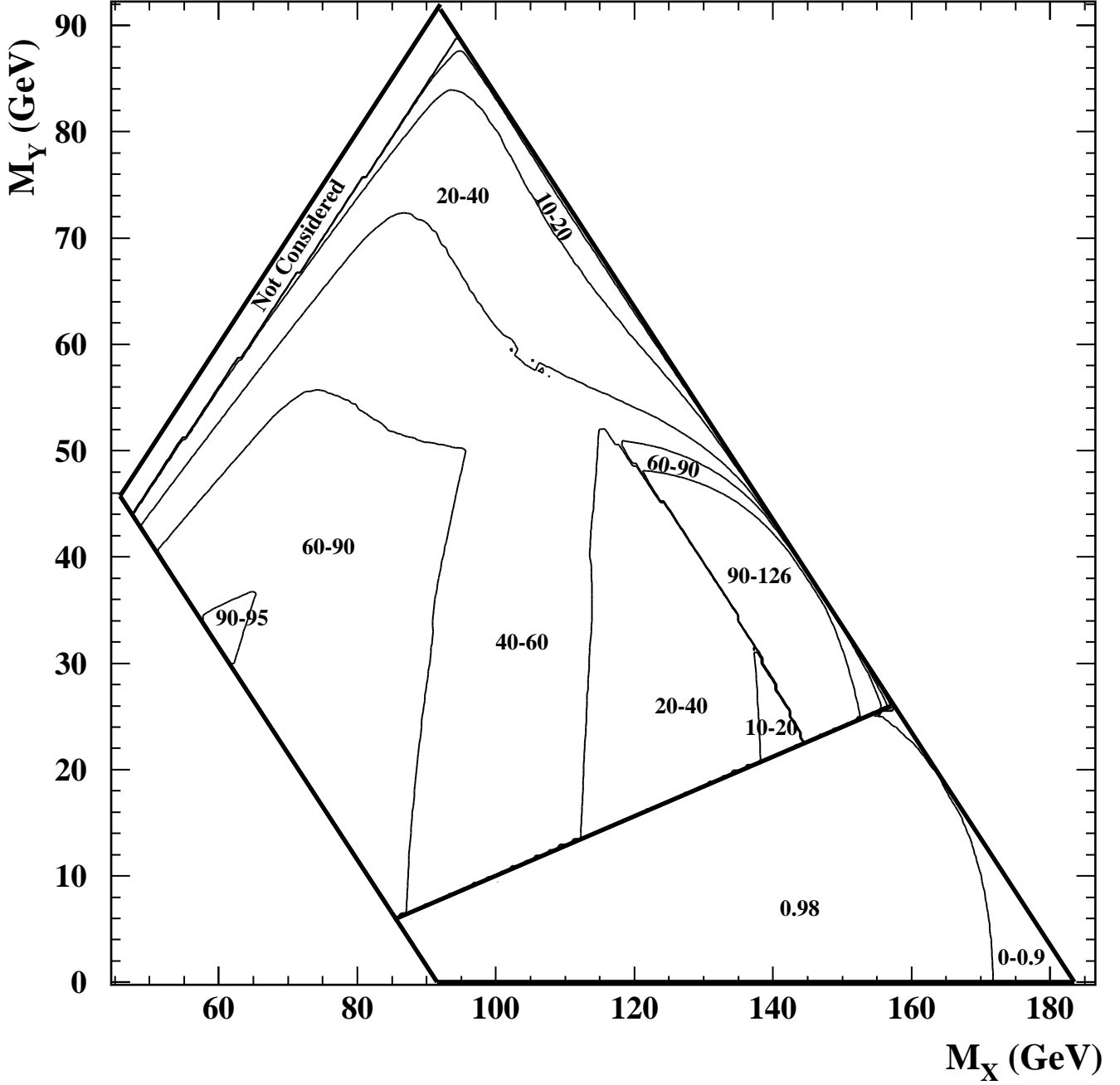
Figure 8: Expected number of single-photon events from the process $e^+e^- \rightarrow \nu\overline{\nu}\gamma(\gamma)$ at $\sqrt{s}$=183 GeV which are consistent with each set of mass values (M_X, M_Y) for the process $e^+e^- \rightarrow XY$, $X \rightarrow Y\gamma$. This figure gives the expected Standard Model contribution to Figure 7. KORALZ was used to model the $e^+e^- \rightarrow \nu\overline{\nu}\gamma(\gamma)$ process. The boundaries and delineated regions are as defined for Figure 6.

OPAL
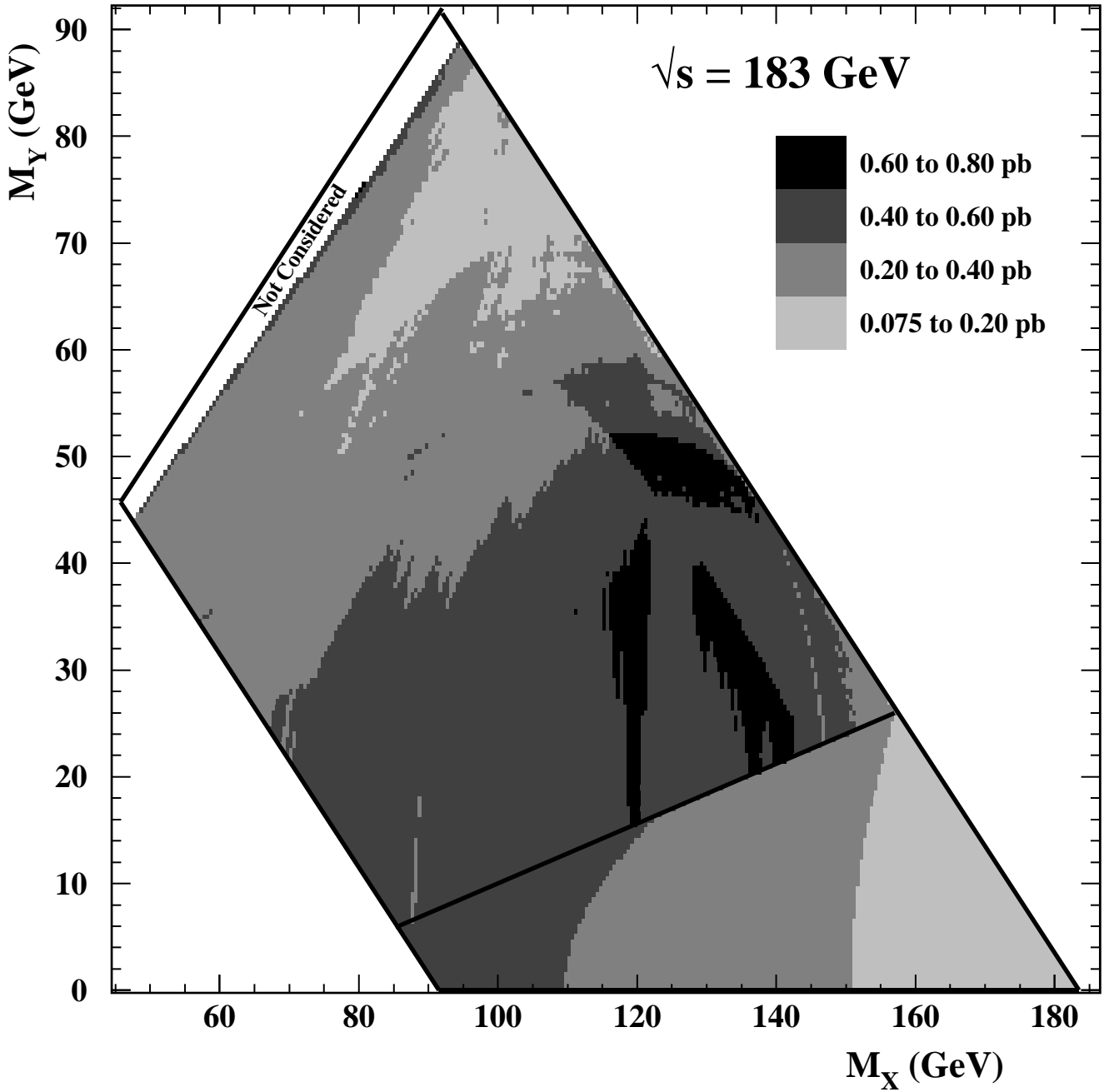
Figure 9: The 95% CL upper limit on $\sigma(e^+e^- \to XY) \cdot BR(X \to Y\gamma)$ at $\sqrt{s} = 183$ GeV as a function of M_X and M_Y. The boundaries and delineated regions are as defined for Figure 6.
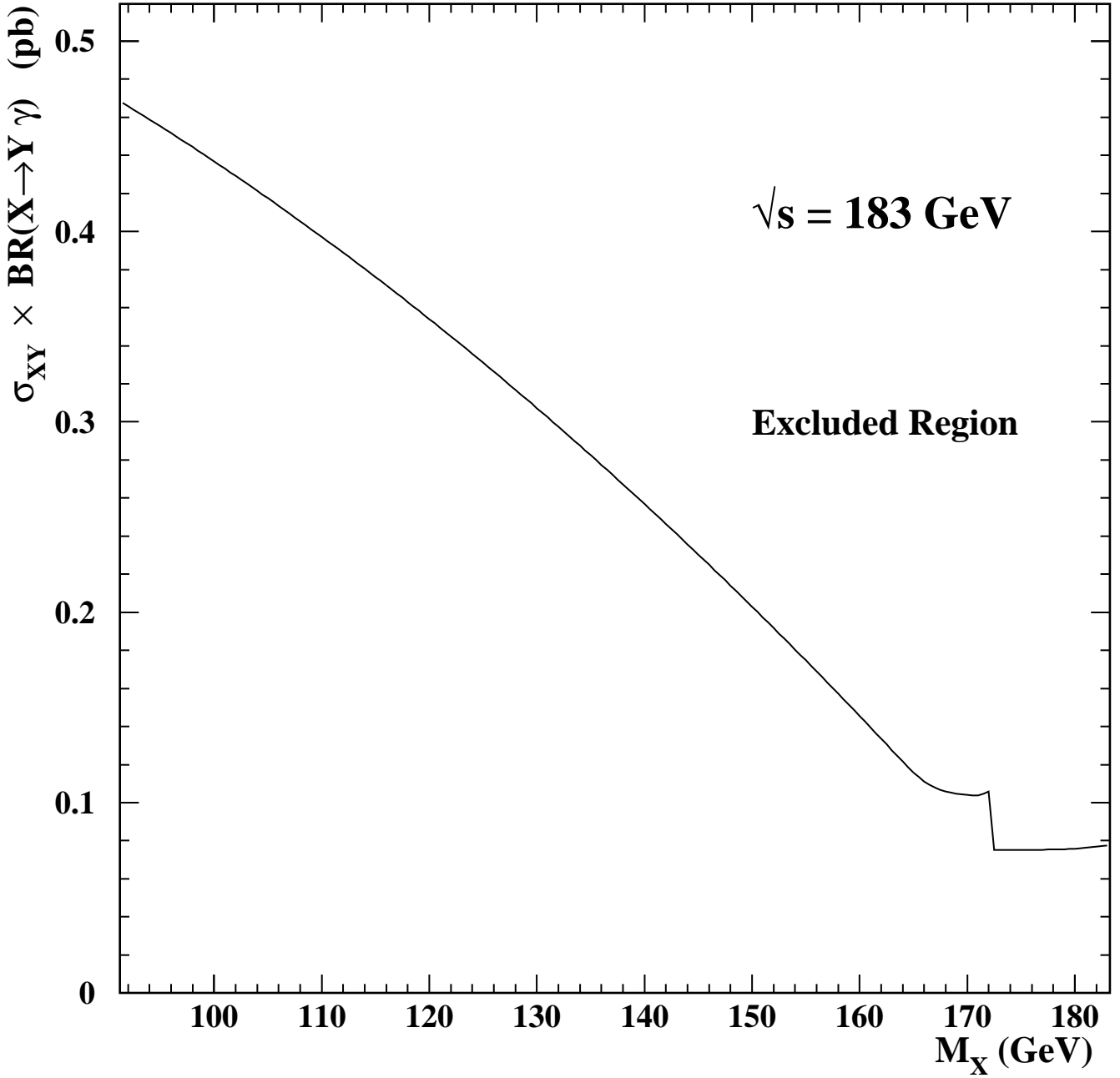
Figure 10: The 95% CL upper limits on $\sigma(\text{e}^+\text{e}^- \to \text{XY}) \cdot \text{BR}(\text{X} \to \text{Y}\gamma)$ at $\sqrt{s} = 183$ GeV as a function of M_X, assuming $M_\text{Y} \approx 0$.

OPAL
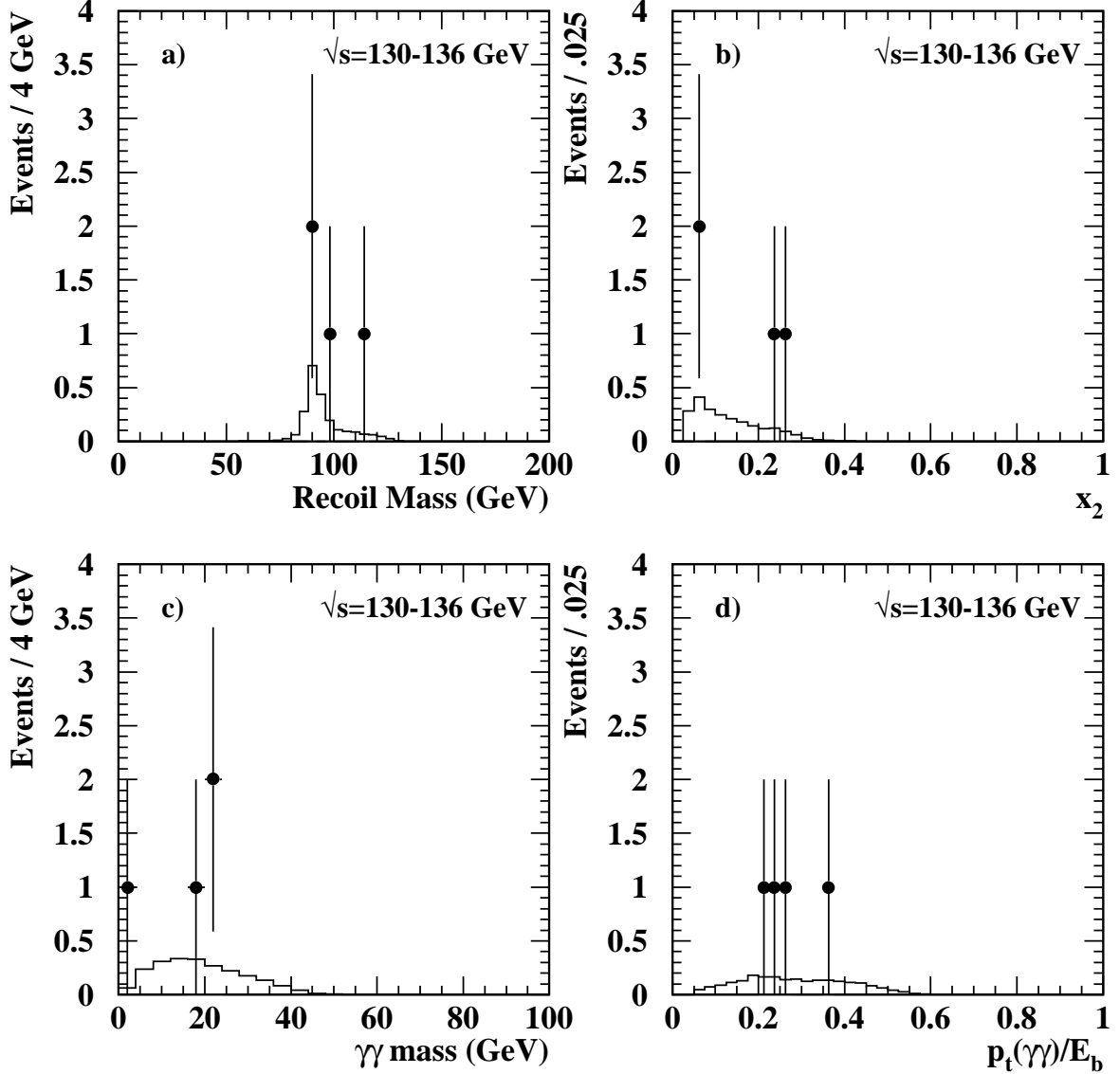
Figure 11: Plots of kinematic quantities for the selected acoplanar-photons events from the combined $\sqrt{s} = 130 - 136$ GeV data sample. a) Recoil mass distribution. b) Distribution of the scaled energy of the second photon (x_2). c) Distribution of the invariant mass of the $\gamma\gamma$ system. d) Scaled transverse energy distribution for the $\gamma\gamma$ system. The data points with error bars represent the selected OPAL data events. In each case the histogram shows the expected contribution from $e^+e^- \rightarrow \nu\bar{\nu}\gamma\gamma(\gamma)$ events, from KORALZ, normalized to the integrated luminosity of the data.
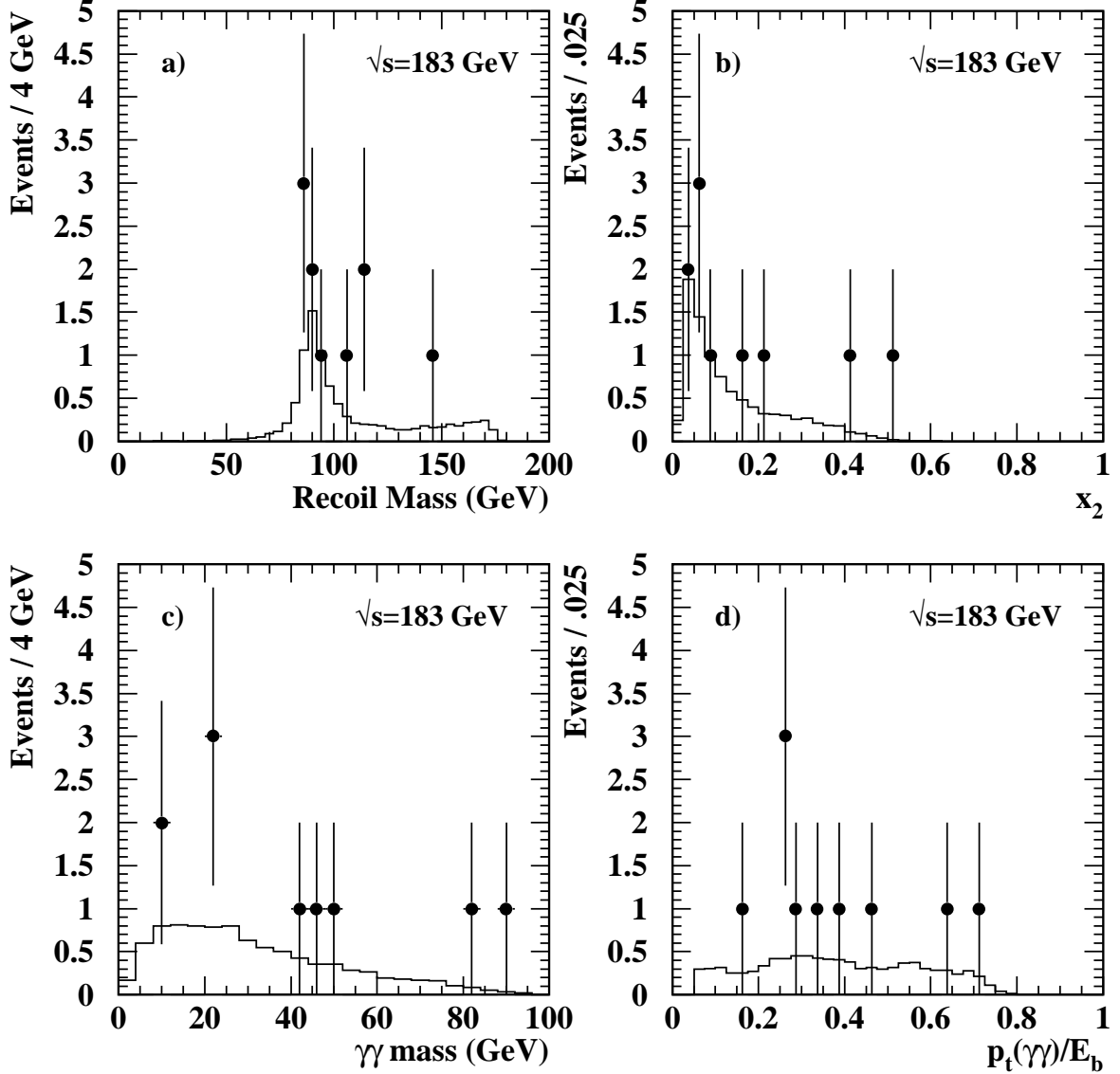
Figure 12: Plots of kinematic quantities for the selected acoplanar-photons events for $\sqrt{s} = 183$ GeV. a) Recoil mass distribution. b) Distribution of the scaled energy of the second photon (x_2). c) Distribution of the invariant mass of the $\gamma\gamma$ system. d) Scaled transverse energy distribution for the $\gamma\gamma$ system. The data points with error bars represent the selected OPAL data events. In each case the histogram shows the expected contribution from $e^+e^- \rightarrow \nu\bar{\nu}\gamma\gamma(\gamma)$ events, from KORALZ, normalized to the integrated luminosity of the data.
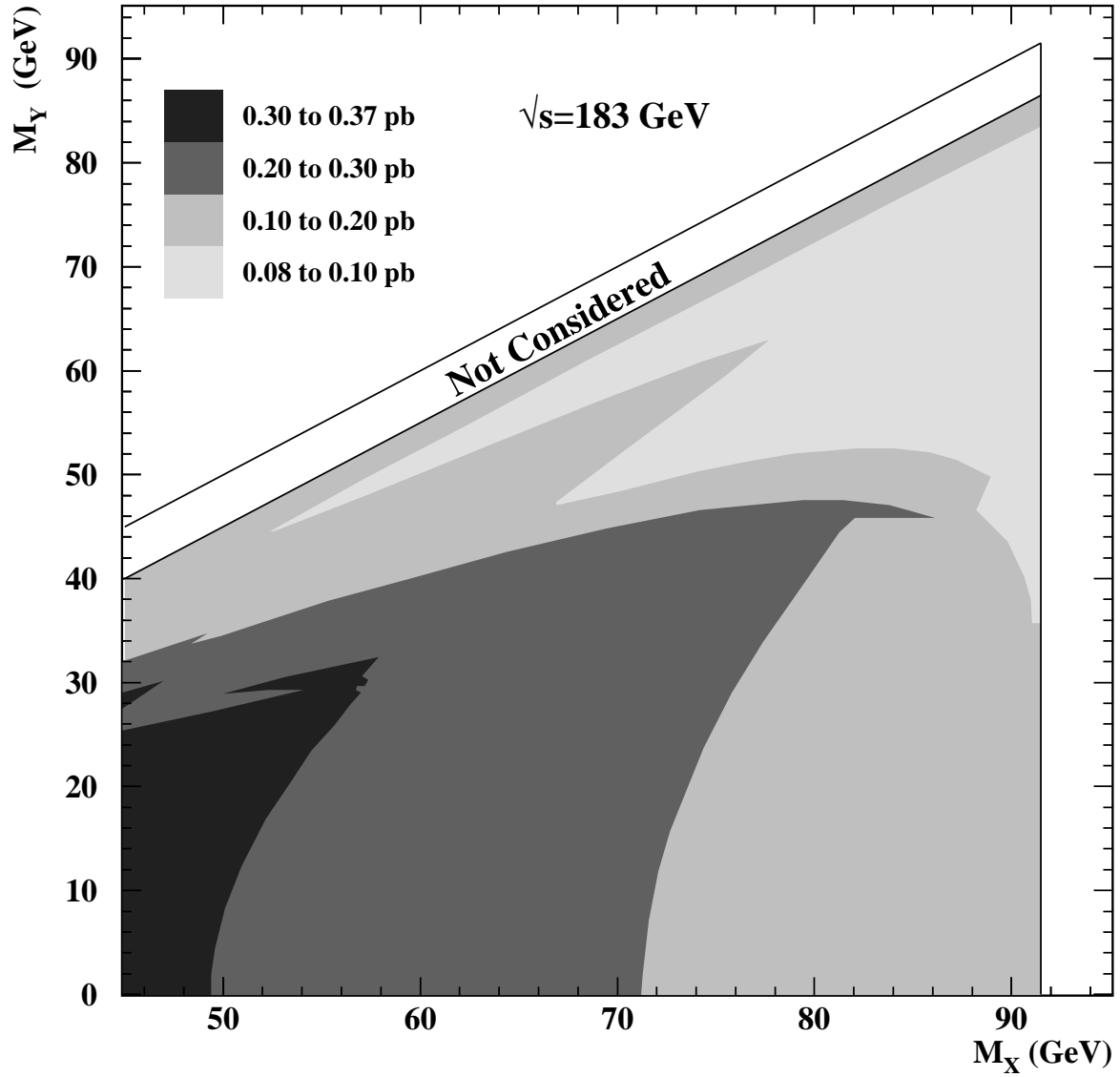
OPAL

Legend:
- 0.30 to 0.37 pb
- 0.20 to 0.30 pb
- 0.10 to 0.20 pb
- 0.08 to 0.10 pb

$\sqrt{s}=183$ GeV

Not Considered

M_Y (GeV)

M_X (GeV)

Figure 13: The shaded areas show 95% CL exclusion regions for $\sigma(e^+e^- \to XX) \cdot BR^2(X \to Y\gamma)$ at $\sqrt{s} = 183$ GeV. No limit is set for mass-difference values $M_X - M_Y < 5$ GeV, defined by the lower line above the shaded regions. The upper line is for $M_X = M_Y$.
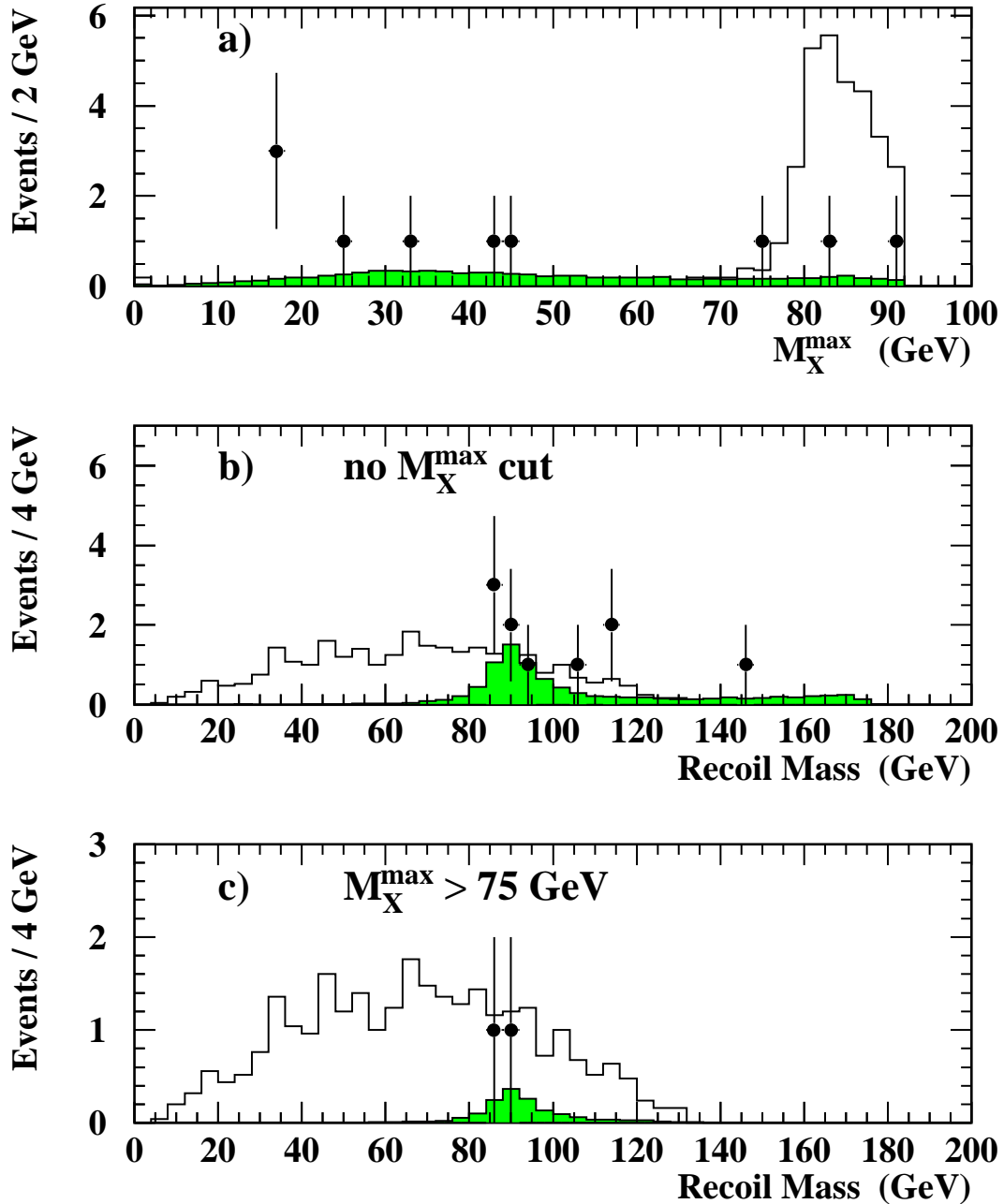
34

OPAL

Figure 14: Properties of selected acoplanar-photons events at $\sqrt{s} = 183$ GeV. a) The M_X^{max} distribution. b) The recoil mass distribution prior to any M_X^{max} requirement. c) The same recoil mass distribution with a cut at $M_X^{max} > 75$ GeV (this cut is for consistency with an M_X of 80 GeV). In each plot the OPAL data are shown as points with error bars, the shaded histogram shows the expected distribution for $e^+e^- \to \nu\bar{\nu}\gamma\gamma(\gamma)$, normalized to the integrated luminosity of the data, and the unshaded histogram shows the expected distribution for the signal process $e^+e^- \to XX$, $X \to Y\gamma$ for $M_X = 80$ GeV. The three distributions for signal Monte Carlo are normalized to the same (arbitrary) production cross-section.

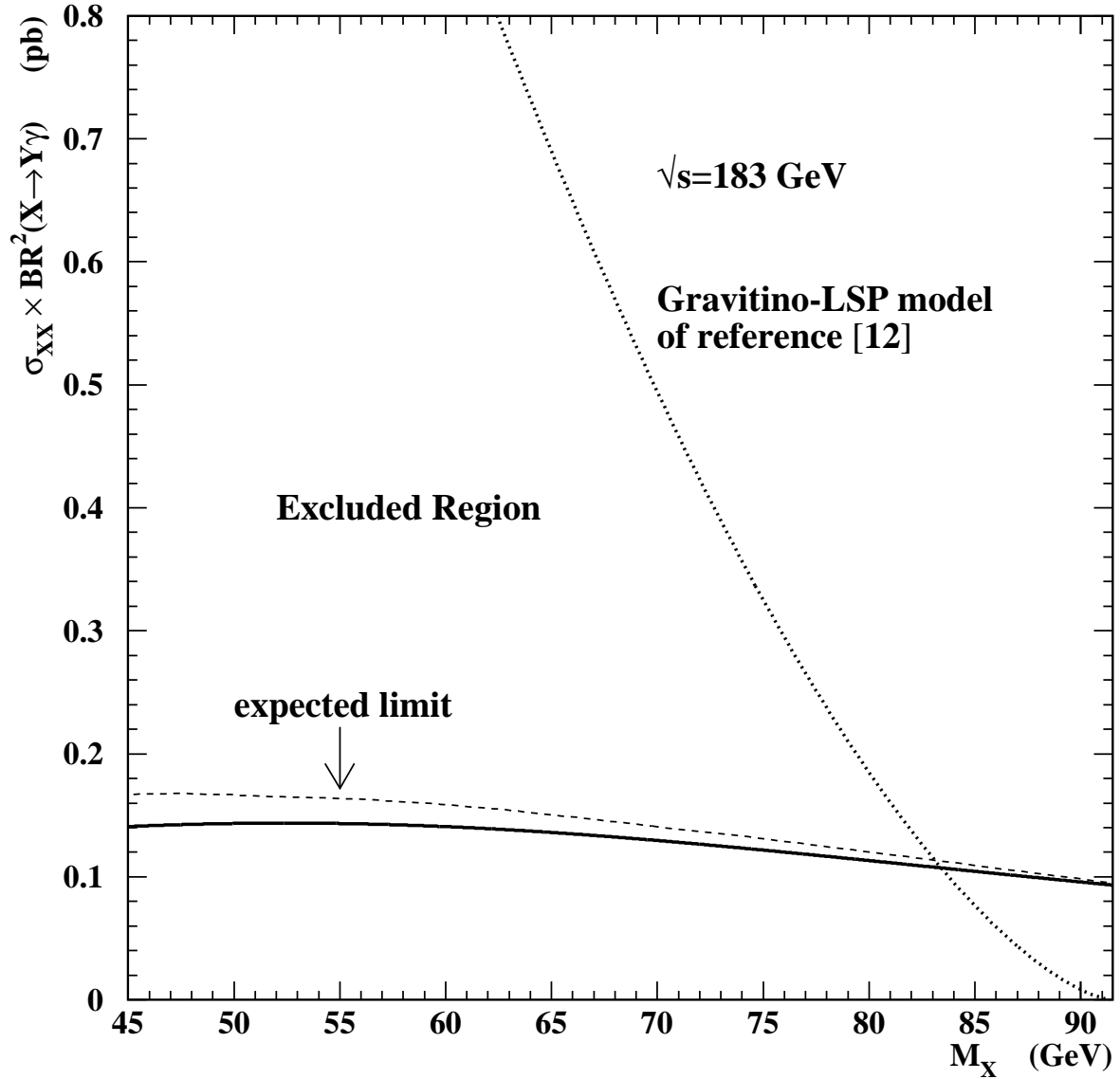Figure 15: 95% CL upper limit on $\sigma(e^+e^- \to XX) \cdot BR^2(X \to Y\gamma)$ for $M_Y \approx 0$ (solid line). Also shown is the expected limit (dashed line). The dotted line shows the cross-section prediction of a specific light gravitino LSP model [12]. Within that model, $\tilde{\chi}_1^0$ masses between 45 and 83 GeV are excluded at the 95% CL. These limits assume that particle X decays promptly.